Transport in Porous Media manuscript No.
(will be inserted by the editor)

Upscaling non-Darcy flow

C.R. Garibotti · M.Peszyńska

Received: date / Accepted: date

Abstract We consider upscaling of non-Darcy flow in heterogeneous porous media. Our approach extends the pressure-based numerical homogenization procedure for linear Darcy flow, due to Durlofsky, to the nonlinear case. The effective coefficients are not constants but rather mildly varying functions of prevailing gradients of pressure. The upscaled model approximates the fine grid model accurately and, in some cases, more accurately than what is expected for Darcy flow; this is due to the non–Darcy effects which suppress heterogeneity. We provide comparisons of alternative approaches as well as consider several variants of numerical realizations of the non–Darcy flow model. Numerical results show effectiveness of the upscaling procedure.

Keywords non-Darcy flow · upscaling · numerical homogenization · finite differences · mixed finite elements

Mathematics Subject Classification (2000) 76S05 · 65N06 · 76M50 · 65N30 · 35B27

1 Introduction

When modeling flow and transport in heterogeneous porous media using numerical methods one often needs to consider a scale H coarser than the h scale at which the data are given. Over the last two or three decades various techniques of *upscaling* from scale h to H, also called *numerical homogenization*, have been defined and critically evaluated, see original papers [14], review [45], and recent work [49,28,8,7]. While methods of upscaling for linear single equation models are reasonably well understood, upscaling nonlinear models or systems, beyond the progress made for multiphase flow [1,17,7], remains, in general, an open field.

Partially supported by National Science Foundation grant 0511190 and Department of Energy grant 98089. Corresponding author: M. Peszynska.

C. Garibotti E-mail: crgaribotti@sinmec.ufsc.br
M. Peszynska E-mail: mpesz@math.oregonstate.edu
Mathematics Department, Oregon State University, Corvallis, OR 97331
Tel.: +1-541-737-9847, Fax: +1-541-737-0517

In this paper we are concerned with upscaling of non-Darcy model of single-phase incompressible fluid flow in saturated porous medium $\Omega \subset \mathbb{R}^d, d = 1, 2, 3$, in the form

$$(\mathbf{K}^{-1} + \beta \mathbf{I}|\mathbf{u}|)\mathbf{u} = -\nabla p. \tag{1}$$

This extends the linear Darcy's law

$$\mathbf{u} = -\mathbf{K}\nabla p, \tag{2}$$

with p denoting pressure or potential, $\mathbf{K}$ denoting the hydraulic conductivity tensor, $\mathbf{I} \in \mathbb{R}^{d\times d}$ the identity matrix and where $\mathbf{u}$ is the velocity (volumetric flux) of the fluid. Here β is the nonnegative scalar known as the Forchheimer coefficient, and the model (1) is due to Forchheimer [25]. Clearly if $\beta = 0$, then (1) reduces to (2). Other formulations are available in literature; we develop these and the notation in Section 2. The conservation of mass is given by

$$\nabla \cdot \mathbf{u} = 0, \tag{3}$$

or, more generally, with a distributed source q by

$$\nabla \cdot \mathbf{u} = q. \tag{4}$$

The central issue addressed in this paper concerns heterogeneous porous media when $\mathbf{K} = \mathbf{K}(\mathbf{x}), \mathbf{x} \in \Omega$. We assume $\beta \equiv const$ or $\beta = \beta(\mathbf{x})$ which occurs for example when β is correlated to $\mathbf{K}$ via some relationship $\beta = g(K)$.

Specifically, the natural question that arises is how to *upscale* the model (1), (3). That is, given values of $\mathbf{K}_h$ and β_h at a scale h, what values of $\mathbf{K}_H$ and β_H should one use in a numerical model at a scale $H >> h$? In particular, if β_h is constant, is it appropriate to assume so for β_H ? Similar questions arise when β_h is not constant but rather correlated to $\mathbf{K}_h$; the answers are not straightforward due to nonlinearity of (1).

For the linear case, that is, Darcy's flow (2)–(3), various *upscaling* and numerical homogenization methods have been shown to be very effective; see [14, 45, 8, 28]. Combine (2) and (3) and consider a numerical approximation on grid parametrized by h of the resulting elliptic PDE, $-\nabla_h \cdot (\mathbf{K}_h \nabla_h p_h) = 0$. Upscaling to scale H means we want to solve $-\nabla_H \cdot (\mathbf{K}_H \nabla_H p_H) = 0$, where the upscaled coefficient $\mathbf{K}_H$ is obtained from one of the known methods; see details in Section 4.

Upscaling of nonlinear models presents a challenge. In particular, consider a nonlinear PDE of the form

$$\nabla \cdot \mathcal{K}(\nabla p_h) = 0,$$

where $\mathcal{K}(\xi_h) = \mathcal{K}(\theta_h; \xi_h)$ is a general nonlinear function of ξ parameterized by some parameters θ, both given at scale h. In general, there is no guarantee that the nonlinearity $\mathcal{K}^*$ in the upscaled model

$$\nabla \cdot \mathcal{K}^*(\nabla p_H) = 0,$$

is parameterized in the same way as $\mathcal{K}$ is in the original model, and even if so, that these parameters are equal to some upscaled θ_H. In other words, in general it is not true that one has $\mathcal{K}^*(\xi_H) = \mathcal{K}(\theta_H;\ \xi_H)$. Rather, to identify $\mathcal{K}^*$, one has to consider a collection of nonlinear upscaled maps; these follow from solutions to local cell problems

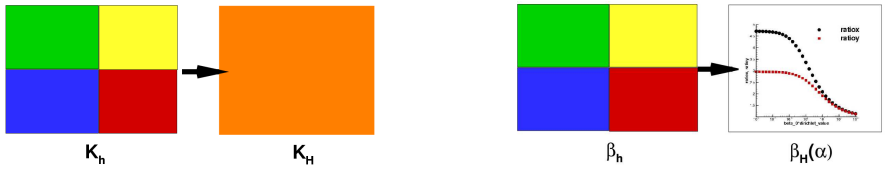

Fig. 1 Schematic difference between linear and nonlinear upscaling. Left: linear upscaling of $\mathbf{K}_h$ delivers a constant upscaled value $\mathbf{K}_H$. Right: nonlinear upscaling of β_h delivers a map $\beta_H(\alpha)$ where α represents a local boundary condition value.

posed at the scale h with cells of size H but in general are not decoupled from the global equation; see [16,7,18]. Additional difficulties in using θ_H arise for systems even if they are linear [40]. See Figure 1 for illustration.

In the problem of interest to this paper, in the nonlinear PDE obtained from (1), (3), we have $\mathcal{K}(\xi_h) = \mathcal{K}(\mathbf{K}_h, \beta_h; \xi_h)$. In what follows we show that upscaling of $\mathcal{K}$ gives a satisfactory upscaled model with $\mathcal{K}^*(\xi_H) = \mathcal{K}(\mathbf{K}_H, \beta_H; \xi_H)$, where the upscaled coefficients $\mathbf{K}_H, \beta_H$ are computed numerically via solutions to cell problems. It turns out that β_H is, in general, not constant but varies midlly with the average flow rates. We focus primarily on pressure-based upscaling after Durlofsky [14].

As a result, we obtain an efficient and accurate method of upscaling (1). We believe that the success of this nonlinear upscaling procedure is due to the fact that the inertia effects appear to supress heterogeneity of $\mathbf{K}$ for large β, which of course helps in the process of upscaling. In addition, we show that in some cases it is reasonable to use a simpler upscaled model with $\mathcal{K}^*(\xi_H) \approx \mathcal{K}(\mathbf{K}_H, \beta_H^g; \xi_H)$ where β_H^g does not require nonlinear upscaling.

Nonlinear upscaling methods with applications to porous media have been applied to multiphase flow problems. There, in addition to deriving $\mathbf{K}_H$, one considers upscaling of nonlinear multiphase flow properties such as saturation-dependent relative permeabilities and/or capillary pressure relationships. The use of *pseudo-functions* [3, 10] is considered an effective yet not always fully satisfactory approach. Difficulty in upscaling multiphase models is associated with large heterogeneity contrasts, with dependence of multiphase flow properties on rock-type, as well as with the nonlinear coupled nature of systems of PDEs that have to be solved. For ongoing research see [8, 7].

On the other hand, there has been considerable research devoted to analysis [24] and numerical approximation [12,36] of non-Darcy flow in homogeneous porous media. To our knowledge, however, not much work has been done for non-Darcy flow in heterogeneous media or devoted to the effects the Forchheimer correction has on the flow in heterogeneous case. In non-Darcy case, the only considerations known to us are in [35] where a scalar case is considered and recent work in [34] where a separate approach applicable to fractured media is considered. In this paper we take a first step towards upscaling of non-Darcy flow for flow driven by boundary conditions only. When $q \not\equiv 0$, for example, when wells are present, non-Darcy flow in homogeneous media was considered in [22]; upscaling around wells for Darcy or for multiphase flow has been considered in [48,11]. Upscaling of non-Darcy flow around wells is outside the present scope.

The plan of the paper is as follows. In Section 2 we give details of the model (1); we also provide analytical bounds and examples which show the connection between $\mathbf{K}, \beta$, and $\mathbf{u}$, and effects of inertia associated with β on heterogeneity. These results help to explain the success of our upscaling procedure to be developed. In Section 3 we define the numerical discretization, with technical details deferred to Appendix. In Section 4 we define our upscaling approach, and in Section 5 we present results of the upscaling method.

Throughout the paper we assume the nondimensional form of (1)–(3) so that $\Omega, \mathbf{K}, \mathbf{u}$ are represented in computational expriments by simple nondimensional quantities. In the presentation we also assume $d = 2$ and $\Omega \ni \mathbf{x} = (x_1, x_2)$ and $\mathbf{u} = (u_1, u_2)$, with natural simplifications or extensions used when $d = 1, 3$. Gravity effects are not included in this paper explicitely, but are easily accounted for in the numerical implementation.

Let $\mathbf{K} = \mathbf{K}(\mathbf{x}), \mathbf{x} \in \Omega$ be a symmetric, bounded, and positive definite uniformly in $\mathbf{x}$ conductivity coefficient. We assume $\mathbf{K}$ is diagonal: $\mathbf{K} = diag(K_1, \dots K_d)$, i.e., the principal axes of permeability variation are aligned with the coordinates $\mathbf{x}$. We note that some pressure-based upscaling methods deliver a non-diagonal $\mathbf{K}_H$ even if the original $\mathbf{K}_h$ is diagonal; however, restriction to diagonal $\mathbf{K}_h$ makes the current exposition manageable, and we drop the off-diagonal terms in $\mathbf{K}_H$, should they arise. Henceforth we assume that each of components satisfies $K_m(\mathbf{x}) \geq \kappa, m = 1, \dots d$ for some $\kappa > 0$. In the isotropic case we have $\mathbf{K} = K\mathbf{I}$.

2 Non-Darcy model, analytical solutions and bounds for (1)

Various formulations of non-Darcy models exist and have been argued as valid in various regimes of flow. In general, it is recognized [20,21,32,4,13] that the non-Darcy flow effects are important in regions of high pressure gradients/ high velocity, and are due to inertia effects, and were originally connected to the onset of turbulence at porescale level. Specifically, for $1 < Re < 100$ the Darcy equation (2) should be replaced by its extended form including additional terms polynomial in velocity modeling inertia.

In most early works an extended model for the scalar case proposed first by Forchheimer [25] was used and validated in the laboratory

$$K^{-1}u + \beta|u|u = -\frac{dp}{dx}. \tag{5}$$

However, there is no uniform agreement on how this equation should be extended to two or three dimensions, how to account for anisotropy, or for multiphase flow. Porescale explanations of non-Darcy phenomena via averaging Navier-Stokes or Oseen flows [47, 31,9,13,33,41] suggest that the form (1) is appropriate, with a possible enhancement of the inertia term to include a full tensor. Our upscaling method does not depend on the particular form of (1) and the form of upscaled β_H suggests a tensor form more general than $\beta\mathbf{I}|\mathbf{u}|$, see Section 5. However, at this point we do not know how succesful our upscaling method is when applied to nonlinearities other than those in (1); this is subject of current and future research.

As concerns heterogeneity of porous media, it is one of its most distinctive properties, and it accounts for difficulties in analysis and numerical simulation not encountered in man-made materials science. Most of the heterogeneity in flow models is reflected by dependence of $\mathbf{K} = \mathbf{K}(\mathbf{x})$. As concerns β, the experiments in which the values of β

were calculated for a given isotropic rock sample suggest that β may be correlated with various powers of K [27]. Also, β is high for carbonate rocks such as limestone and sandstone and generally higher for vugular than for non-vugular rocks [30]. In general, it is reasonable to conclude that in heterogeneous nonisotropic porous media, $\beta = \beta(\mathbf{x})$ whenever $\mathbf{K} = \mathbf{K}(\mathbf{x})$.

In this paper we report, for simplicity, only on two variants of β, indexed by $\mathcal{B}$, which for isotropic $\mathbf{K} = K\mathbf{I}$ read

$$\beta = g_{\mathcal{B}}(\beta_0, K) = \begin{cases} \beta_0, & \mathcal{B} = 0 \\ \frac{\beta_0}{\sqrt{K}}, & \mathcal{B} = 1 \end{cases}. \tag{6}$$

More [27,30] can be easily incorporated. However, a special case of non-smooth g such as the one for fracture systems where inertia terms are neglected in the matrix, will not be considered here but is a topic of future work. See also Section 5.3.4 on our computational results regarding correlation. In general β may actually vary with pressure and/or composition of fluids, and some formulations of (1) account for this [12,23,24,22]. For simplicity throughout this paper we consider a fixed single phase fluid and, hence, we lump the viscosity and density coefficients along with $\mathbf{K}, \beta$.

For nonisotropic diagonal $\mathbf{K}$ the correlations (6) should be considered componentwise; we find it therefore natural to allow for $\beta = (\beta_1, \beta_2)$ to be a vector. Non-isotropic β may also arise in the process of upscaling; a vector form of β does not introduce additional difficulties in a numerical model. With this, we rewrite (1) componentwise, with the coupling term between components given by $|\mathbf{u}| = \sqrt{\sum_{m=1}^{d} u_m^2}$,

$$(K_m^{-1} + \beta_m|\mathbf{u}|)u_m = -\frac{\partial p}{\partial x_m},\ m = 1, \dots d. \tag{7}$$

A simplified version, in which the nonlinearity in velocity components is decoupled, is the one adapted in [22], and it is a multi-dimensional analogue of (5),

$$(K_m^{-1} + \beta_m|u_m|)u_m = -\frac{\partial p}{\partial x_m},\ m = 1, \dots d. \tag{8}$$

Since (7) is more general, it will be used as a basis for numerical models. Interestingly, in some numerical discretizations, a discrete version of (8) arises on its own from discretization of (7).

2.1 Analytical solution and bounds

It is not difficult to find an analytical solution u to (5). In the multidimensional case, it may no more be directly possible. Below we derive bounds which are helpful in scalar and non-scalar cases.

2.1.1 Estimates for scalar case

Let $D = -\frac{dp}{dx}$. Rewrite (5) as

$$u = \mathcal{K}(D), \tag{9}$$

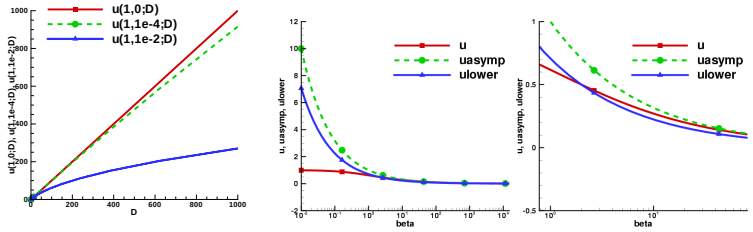

Fig. 2 Analytical solution $u = \mathcal{K}(K, \beta; D)$. Left: we show $\mathbf{u} = \mathcal{K}(1, \beta; D)$ for a fixed β in function of D. Note the deviation of non-Darcy velocity from linear Darcy velocity ($\beta = 0$). Middle and right: plot of $u = \mathcal{K}(1, \beta; 1)$ versus β and zoom of the figure. Both exact values and asymptotic bounds are shown.

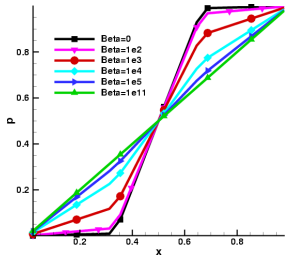

Fig. 3 Effects of inertia on heterogeneity. Shown is pressure solution for cross flow in a layered medium where K varies from 1 (left and right) to 10^{-4} in the middle part, for various values of β. Notice a sharp jump of pressure gradient for the case $\beta = 0$; the jump becomes smaller with larger β.

where $\mathcal{K}(D) = \mathcal{K}(K, \beta; D)$. Solving (5) gives the following

$$u = \mathcal{K}(K, \beta; D) = \begin{cases} 0, & D = 0, \\ KD, & \beta = 0, \\ sgn(D)\frac{-K^{-1}+\sqrt{(K^{-1})^2+4\beta|D|}}{2\beta}, & \beta \neq 0, D \neq 0, \end{cases} \tag{10}$$

where $sgn(D)$ denotes the sign of D. One can also write

$$u = \mathcal{K}(K, \beta; D) = \frac{2D}{K^{-1} + \sqrt{(K^{-1})^2 + 4\beta|D|}}, \tag{11}$$

from which it readily follows that $\mathcal{K}(K, \beta; D)$ is continuous in all arguments and parameters. Also, $\mathcal{K}$ is increasing in D but decreasing in β. See Figure 2 for typical behavior of $u = \mathcal{K}(K, \beta; D)$. The calculation

$$\frac{\partial \mathcal{K}}{\partial D} = \frac{sgn(D)}{\sqrt{(K^{-1})^2 + 4|D|\beta}} \tag{12}$$

with $\frac{\partial \mathcal{K}}{\partial D}|_{\beta=0} = K$ for Darcy flow, is useful in Jacobian; see Sections 3 and 7.1.

2.1.2 Bounds for u

An expression equivalent to (11) is

$$u = \mathcal{K}(K, \beta; D) = sgn(D)\left(-c + \sqrt{c^2 + \frac{|D|}{\beta}}\right), \quad c = \frac{K^{-1}}{2\beta}, \quad \beta \neq 0. \tag{13}$$

Clearly, since $-c + \sqrt{c^2 + \frac{|D|}{\beta}} \leq KD$, we have $\mathcal{K}(D) \leq KD$; i.e., the non-Darcy velocities do not exceed the Darcy velocities for the same pressure gradients. We recall that $\mathcal{K}^{-1}$ is sometimes called *a resistance parameter* which grows with increasing β or $|u|$ [13].

On the other hand, from $\frac{1}{\sqrt{2}}(r+q) \leq \sqrt{r^2+q^2} \leq r+q$ for any $r, q \geq 0$, we see that, for $\beta \neq 0$

$$\mathcal{K}(K, \beta; D) \leq \sqrt{\frac{|D|}{\beta}} \tag{14}$$

$$\mathcal{K}(K, \beta; D) \geq \sqrt{\frac{|D|}{2\beta}} - \frac{K^{-1}}{2\beta}(1 - \frac{1}{\sqrt{2}}) \tag{15}$$

and that for large $\beta \geq \beta_{crit} = \frac{2}{|D|K^2}$, one actually has

$$\mathcal{K}(K, \beta; D) \geq \sqrt{\frac{|D|}{2\beta}}, \ \beta \geq \beta_{crit}. \tag{16}$$

For $\beta \geq \beta_{crit}$, since $\mathcal{K}(K, \beta; D)$ decreases with β, we additionally have

$$\mathcal{K}(K, \beta; D) \leq \mathcal{K}(K, \beta_{crit}; D) = \frac{DK}{2}, \quad \beta \geq \beta_{crit}. \tag{17}$$

These bounds are useful in numerical calculations since they help to select a good initial guess for a local nonlinear solver.

More importantly, we obtain the asymptotics for large β which follows from (14), (16),

$$u = \mathcal{K}(K, \beta; D) \approx \theta\sqrt{\frac{|D|}{\beta}}, \quad \theta \approx 1. \tag{18}$$

This approximation is quite revealing; it demonstrates that for really large inertia effects, the flux u is *essentially independent* of K. While u computed for realistic values of K, β, D found in porous media may not necessarily be in this asymptotic regime, (18) shows that the qualitative nature of u may be only mildly affected by heterogeneity of K, if large inertia effects are present. This is illustrated by numerical experiments shown in Figure 3 where we see that with increasing β one obtains more smoothing of $\frac{dp}{dx}$.

For a given boundary condition, one can solve for p by integrating (10); we skip the calculation. This is not in general possible for the nonscalar case.

It is convenient to define the transmissibility [37]

$$\mathcal{T}(K, \beta, \gamma, u) = \frac{1}{K^{-1} + \beta\sqrt{\gamma^2 + u^2}}, \tag{19}$$

and rewrite (5) in an implicit form as

$$u = \frac{D}{K^{-1} + \beta|u|} = \mathcal{T}(K, \beta, 0, u)D. \tag{20}$$

2.1.3 Non-scalar case

Now we set $D_m = -\frac{\partial p}{\partial x_m}$, and use $\gamma^2 = \sum_{n\neq m}(u_n)^2$ which combines all components of velocity other than m, and we rewrite (7)

$$\left(K_m^{-1} + \beta_m \sqrt{\gamma^2 + (u_m)^2}\right) u_m = D_m. \tag{21}$$

We then have

$$u_m = \mathcal{T}\left(K_m, \beta_m, \sqrt{\sum_{n\neq 2} u_n^2}, u_m\right) D_m.$$

Note that $\mathcal{T}(K_m, \beta_m, \sqrt{\sum_{n\neq 2} u_n^2}, u_m) = \mathcal{T}(K_m, \beta_m, 0, |\mathbf{u}|)$; this simplifies the forthcoming numerical calculations discussed in Section 7.1.

Given $(u_n)_{n\neq m}$, that is, γ, one can find u_m explicitly from (21) and/or derive estimates similar to those for the scalar case. In general of course, γ itself is unknown. However, given $D_m, m = 1, \dots d$, one can solve (21) by fixed point or Newtonian iteration. Difficulties arise in numerical calculations because the discrete form of (21) involves a large stencil; see Sections 3 and 7.2.

3 Numerical discretization

Here we formulate a discrete version of (3) and (1) as a cell-centered finite difference method (CCFD) in several variants depending on discretization of $|\mathbf{u}|$ in (7). These variants and discretization are motivated using mixed Finite Elements in Section 7.2; this development has a theoretical value in that the convergence results proved in [36] for mixed FE methods apply to our discretization. Additionally, we obtain insight into why a particular discrete version of (7) is justified. From the point of view of upscaling, we show later that all the variants behave similarly; in other words, the success of upscaling is not tied to a particular variant of discretization.

Let the region Ω be decomposed into rectangular *elements* or *cells* Ω_{ij} on a Cartesian grid with natural notation of $\mathbf{x}_{ij} = (x_{1,ij}, x_{2,ij})$ denoting cell centers. The elements Ω_{ij} are of size $\triangle x_i \times \triangle y_j$. The edge $E_{i+1/2,j}$ between Ω_{ij} and $\Omega_{i+1,j}$ has a center at $(x_{1,i+1/2,j}, y_j)$, and so on. The distances between cell centers are denoted by $\triangle x_{i+1/2,j}$ etc.. The parameter h is the maximum of either $\triangle x_i, \triangle y_j$. When coarse grid with parameter H is used, we index the cells using I, J.

The discrete pressures $p_h \equiv (p_{ij})_{i,j=1}$ are associated with cell centers. The normal components of velocities are associated with midpoints of cell edges; on the cell Ω_{ij} the velocity in direction x_1 is defined by its values $u_{1,i-1/2,j}$ on the left and $u_{1,i+1/2,j}$ on the right edges. The discrete velocities $\mathbf{u}_h$ can be then considered to be a tensor product of piecewise linear polynomials in x_1 direction and piecewise constant polynomials in the x_1 direction and opposite in the x_2 direction. The notation is standard; see [37,46, 6] for details.

Recall [37,46] the standard discrete counterpart of (3)

$$\nabla_h \cdot \mathbf{u}_h = 0, \tag{22}$$

and of (2), which we develop now. In the direction x_1 we have

$$u_{1,i+1/2,j} = K_{1,i+1/2,j} \frac{p_{i,j} - p_{i+1,j}}{\triangle x_{i+1/2,j}} = T_{1,i+1/2,j} \left(p_{i,j} - p_{i+1,j} \right), \tag{23}$$

where transmissibility $T_{1,i+1/2,j} = \frac{K_{1,i+1/2,j}}{\triangle x_{i+1/2,j}}$ is defined, and harmonic averaging of permabilities is used [37]:

$$K^{-1}_{1,i+1/2,j} = \frac{1}{2 \triangle x_{i+1/2,j}} \left(K^{-1}_{1,ij} \triangle x_i + K^{-1}_{1,i+1,j} \triangle x_{i+1} \right). \tag{24}$$

3.1 Discrete non-Darcy velocities

With notation as above, we can now state the following discrete counterpart of (1) or (7), with mixed finite element derivation deferred to Section 7.2:

$$\left(T^{-1}_{1,i+1,j} + \frac{1}{2} \left(\beta_{1,ij} \triangle x_i |\mathbf{u}_h|^+_{i,j} + \beta_{1,i+1,j} \triangle x_{i+1} |\mathbf{u}_h|^-_{i+1,j} \right) \right) u_{1,i+1/2,j} = p_{i,j} - p_{i+1,j}. \tag{25}$$

An analogous definition can be written immediately in direction x_2.

The crucial point is to define the terms $|\mathbf{u}_h|^+_{i,j}$ and $|\mathbf{u}_h|^-_{i+1,j}$. These have the meaning of magnitude of velocity on the cells i, j and $i+1, j$, respectively, each relative to the edge $E_{i+1/2,j}$ on which the velocity component $u_{1,i+1/2,j}$ is being defined. They can be defined in several ways, which we denote below as variants $\mathcal{V} = 0, 1, 2, 3$.

Consider $|\mathbf{u}_h|^+_{i,j}$, with $|\mathbf{u}_h|^-_{i,j}$ defined analogously. The simplest way to define it ($\mathcal{V} = 0$) is to use the magnitude of normal component of $\mathbf{u}_h$ on the edge $E_{i+1/2,j}$ that is, $|u_{1,i+1/2,j}|$, as was done in [22].

Another way, $\mathcal{V} = 2$, is to use the magnitude of $\mathbf{u}_h$ itself on the edge $E_{i+1/2,j}$ which is defined using

$$(\bar{\mathbf{u}}_h)^+_{ij} = \left(u_{1,i+1/2,j}, \frac{u_{2,i,j+1/2} + u_{2,i,j-1/2}}{2} \right)$$
$$(\bar{\mathbf{u}}_h)^-_{ij} = \left(u_{1,i+1/2,j}, \frac{u_{2,i+1,j+1/2} + u_{2,i+1,j-1/2}}{2} \right),$$

or, with the quantity ($\mathcal{V} = 1$),

$$(\bar{\mathbf{u}}_h)_{ij} = \frac{(\bar{\mathbf{u}}_h)^+_{ij} + (\bar{\mathbf{u}}_h)^-_{ij}}{2}.$$

Finally, the most general way, called $\mathcal{V} = 3$, is to use the magnitude(s) of (interpolated) value(s) of

$$(\mathbf{u}_h)_{ij} = \left(\frac{u_{1,i+1/2,j} + u_{1,i-1/2,j}}{2}, \frac{u_{2,i,j+1/2} + u_{2,i,j-1/2}}{2} \right),$$
$$(\mathbf{u}_h)_{i+1,j} = \left(\frac{u_{1,i+1/2,j} + u_{1,i+3/2,j}}{2}, \frac{u_{2,i+1,j+1/2} + u_{2,i+1,j-1/2}}{2} \right),$$

in the middle of cells Ω_{ij} and $\Omega_{i+1,j}$, respectively.

Summarizing, we define

$$|\mathbf{u}_h|^+_{i,j} = \begin{cases} |u_{1,i+1/2,j}|, & \text{variant} = 0, \\ |(\bar{\mathbf{u}}_h)_{ij}|, & \text{variant} = 1, \\ |(\bar{\mathbf{u}}_h)^+_{ij}|, & \text{variant} = 2, \\ |(\mathbf{u}_h)_{ij}|, & \text{variant} = 3. \end{cases} \tag{26}$$

These four variants lead to somewhat different numerical solutions to (1)-(3).

Variant $\mathcal{V} = 0$ is a direct discretization of (8); it can also be seen as a simplification/approximation of variants $\mathcal{V} = 1, 2$. It uses the same 5-point stencil as used for Darcy' law with diagonal $\mathbf{K}$ and allows for analytical component-wise resolution of local nonlinearities.

Variants $\mathcal{V} = 1, 2, 3$ are associated each with a different method of numerical integration in mixed FE applied to (7); see Section 7.2. The difference between $\mathcal{V} = 1$ and $\mathcal{V} = 2$ is not larger than the one appearing in the use of numerical quadrature to derive (23) from (2) using mixed FE. Both variants couple the velocity $u_{1,i+1/2,j}$ to four other velocity degrees of freedom, and are equivalent to each other up to higher order terms; see Section 7.2. With $\mathcal{V} = 1$ we have symmetry in that $|\mathbf{u}_h|^+_{i,j} = |\mathbf{u}_h|^-_{i+1,j}$, and one can get around the difficulty of an enlarged stencil when resolving local nonlinearities, by iteration-lagging those components in $|(\bar{\mathbf{u}}_h)_{ij}|$ other than $u_{1,i+1/2,j}$. Variant $\mathcal{V} = 2$ is somewhat more complicated than $\mathcal{V} = 1$, because $|\mathbf{u}_h|^+_{i,j}$ is not identical to $|\mathbf{u}_h|^-_{i,j}$.

Variant $\mathcal{V} = 3$ is the most complex one, and, if applied in (25) alone, it couples velocity $u_{1,i+1/2,j}$ and pressures $p_{i,j}, p_{i+1,j}$ to 6 other velocity degrees of freedom appearing in its definition and thereby to 6 additional pressure values. The stencil in the resulting discrete system is increased from 5-point to 13-point in $d = 2$. In addition, resolution of local nonlinearity is not very succesful by iteration lagging and impossible directly. While we performed numerical experiments with this variant, its complexity is not offering promise of being a succesful model.

In view of the above, only $\mathcal{V} = 0, 1$ will be discussed further. In summary then, discretization of (7) or (8) takes the form

$$\left(T^{-1}_{1,i+1,j} + B_{1,i+1/2,j}|(\mathbf{u}_h)^{\mathcal{V}}_{i+1/2,j}|\right) u_{1,i+1/2,j} = p_{i,j} - p_{i+1,j}, \tag{27}$$

where we define $B_{1,i+1/2,j} = \frac{1}{2}\left(\beta_{1,ij} \triangle x_i + \beta_{1,i+1,j} \triangle x_{i+1}\right) = \triangle x_{i+1/2}\beta_{1,i+1/2,j}$, and where $|(\mathbf{u}_h)^{\mathcal{V}}_{i+1/2,j}|$ is computed according to (26).

It is convenient to cast (27) in a form similar to (23) and (20). Define the transmissibilities $\Upsilon^{\mathcal{V}}_{1,i+1/2,j}$ which, unlike $T_{1,i+1/2,j}$, depend nonlinearly on the solution,

$$\Upsilon^{\mathcal{V}}_{1,i+1/2,j} = \mathcal{T}(T_{1,i+1/2,j}, B_{1,i+1/2,j}, 0, |(\mathbf{u}_h)^{\mathcal{V}}_{i+1/2,j}|), \tag{28}$$

with a similar definition for $\Upsilon_{2,i,j+1/2}$. Now (27) reads, for every i, j

$$u_{1,i+1/2,j} = \Upsilon^{\mathcal{V}}_{1,i+1/2,j}(p_{i,j} - p_{i+1,j}), \tag{29}$$

$$u_{2,i,j+1/2} = \Upsilon^{\mathcal{V}}_{2,i,j+1/2}(p_{i,j} - p_{i,j+1}), \tag{30}$$

and in a vector form we can write symbolically, for $\mathbf{u}_h = \left((u_{1,i+1/2,j}, u_{2,i,j+1/2})\right)_{ij}$,

$$\mathbf{u}_h = \mathbf{T}^{\mathcal{V}}\left(\mathbf{K}_h, \beta_h, |\mathbf{u}_h|, \mathbf{u}_h\right) \nabla_h p_h = \mathbf{T}^{\mathcal{V}}_h \nabla_h p_h. \tag{31}$$

Note finally that if $\beta \equiv 0$ we have $\mathbf{T}^{\mathcal{V}}(\mathbf{K}_h, 0, |\mathbf{u}_h|, \mathbf{u}_h) \equiv -\mathbf{K}_h$. Also, recall that if $\mathcal{V} = 0$, the implicit relationships (29) and (30) can be resolved explicitely.

This formulation is used in the remainder of this paper; see Section 7.2 for mixed FE derivation and Section 7.1 for details of nonlinear solver. Also, see Section 5 for discussion of the difference between variants $\mathcal{V} = 0, 1$. To complete this Section, we comment on boundary conditions.

3.1.1 Boundary conditions

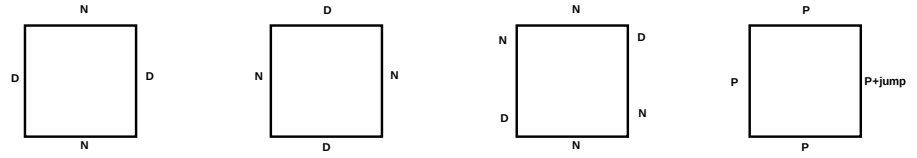

Fig. 4 Boundary conditions used in examples and upscaling procedures

In examples and upscaling procedures discussed in this paper we consider one of the following types of boundary conditions, represented schematically in Figure 4.

Let us be given Γ_D, Γ_N which denote the Dirichlet and Neumann no-flow parts of the boundary $\partial\Omega$, respectively. We impose

$$p|_{\Gamma_D} = p_D \tag{32}$$

$$\mathbf{K}\nabla p \cdot \nu|_{\Gamma_N} = 0. \tag{33}$$

Examples of Γ_D, Γ_N for a rectagular domain Ω denoted B1, B2, B3, and used in examples in Section 5 are shown in Figure 4. Of course, other arrangements are possible.

In the numerical model, we apply Dirichlet boundary conditions using an algorithm shown in [42,39]. The no-flow Neumann conditions are natural for CCFD and are equivalent to setting transmissibilities on appropriate edges to 0 [37].

For a rectangular domain Ω, instead of Dirichlet and Neumann conditions, one may choose to apply periodic boundary conditions (BP). Here we dicern between oppposite sides of the rectangular domain, say Γ_- and Γ_+, and impose

$$p|_{\Gamma_+} = p|_{\Gamma_-} + \text{ jump} \tag{34}$$

$$\mathbf{K}\nabla p \cdot \nu|_{\Gamma_+} = -\mathbf{K}\nabla p \cdot \nu|_{\Gamma_-}. \tag{35}$$

Here the jump may be equal to 0, or not; usually exactly one of the sides (left or right, top or bottom) will have a nonzero jump.

Implementation of periodic boundary conditions of the type (BP) shown in Figure 4 is done by introducing an additional set of unknowns $p_{\partial\Omega}$. These unknowns play a dual role: first, they are used as the *known* values of "Dirichlet data". Second, their values on opposite sides of the domain are either matched or are subject to a prescribed jump. Finally, to close the system, the fluxes on opposite sides are matched. The system as such is underdetermined and one has to add an additional condition which fixes the average of p_h over Ω. In implementation one can eliminate the additional unknowns $p_{\partial\Omega}$.

4 Upscaling

This section provides answers to the core issues addressed in this paper. Let us be given a scale h, identified as diameter of Ω_{ij}, on which the coefficients $\mathbf{K}_h, \beta_h$ are given, but at which it is practically impossible to solve the system (53). Assume there is a coarse scale $H >> h$ at which such computations are possible. The main issue is to find the equations which describe the problem at scale H, and to identify their coefficients. Our premise is that this is possible and that an upscaled version of (53)

$$\nabla_H \cdot \mathbf{T}_H^{\mathcal{V}} \nabla_H p_H = 0 \tag{36}$$

can be identified.

Alternatively, one can use a numerical method at scale H which incorporates the variation of $\mathbf{K}_h$ in its *definition*; this is done in subgrid upscaling or multiscale and variational approaches to Finite Element methods; see [2,19,15,18,17] and related work. Yet another alternative is to use mortar upscaling [42].

Our approach in this paper in using (36) is traditional, and we aim to derive $\mathbf{K}_H, \beta_H$ from $\mathbf{K}_h, \beta_h$. We briefly review what was done for Darcy flow and then proceed to non-Darcy case.

4.1 Upscaling $\mathbf{K}_h$ and notation

For Darcy flow it is standard to consider the upscaled linear system at scale H to be of the same form as the one at h, which is also linear. Various methods M of upscaling $(\mathbf{K})_h \mapsto (\mathbf{K})_H$ have been reviewed in [45]; these include arithmetic $M = A$ or harmonic $M = \mathcal{H}$ averaging and give $(\mathbf{K})_H^A$, $(\mathbf{K})_H^{\mathcal{H}}$, respectively. The *pressure-based* methods [14] which deliver $(\mathbf{K})_H^D$,$(\mathbf{K})_H^P$ and use Dirichlet and periodic boundary conditions, respectively, perform better than $M = A, \mathcal{H}$ but are more computationally expensive. They are related to homogenization methods pursued in mathematical analysis [5].

Here we briefly recall the method proposed in [14]. Fix a grid cell Ω_{IJ} at scale H. By upscaling Darcy flow coefficients, we want to ensure that (23) holds on the grid H. Since (23) is linear, it is natural to ask that the fluxes on grid H which arise due to pressure gradients imposed on that grid, agree *on average* with fluxes on grid h, when these arise from the same global pressure gradients; this requirement preserves mass. With this approach, one finds $\mathbf{K}_H|_{\Omega_{IJ}}$ by inverse modeling as the appropriate coefficient of proportionality. The caveat is that one has to solve a cell problem on Ω_{IJ} subject to some global pressure gradients in order to compute that response. How these pressure gradients are imposed determines the D and P methods.

Consider first the local cell problem with Dirichlet boundary conditions of type B1, see Figure 4. We solve for $\tilde{p}_h, \tilde{u}_h$

$$-\nabla_h \cdot (\mathbf{K}_h \nabla_h \tilde{p}_h) = 0, \quad \mathbf{y} \in \Omega_{IJ} \tag{37}$$

$$\tilde{p}|_{\Gamma_{1,I-1/2,J}} = 0 \tag{38}$$

$$\tilde{p}|_{\Gamma_{1,I+1/2,J}} = D_{I,J} \tag{39}$$

$$(\mathbf{K}_h \nabla \tilde{p} \cdot \mathbf{n})|_{\Gamma_{2,I,J+1/2} \cup \Gamma_{2,I,J-1/2}} = 0. \tag{40}$$

Then we compute the total flux $\tilde{u}_{1,I+1/2,J} = \int_{\Gamma_{1,I,J+1/2}} \tilde{u}_h \cdot \mathbf{n}$, and we find $K^D_{1,I+1/2,J}$ by fitting it into the counterpart of (23)

$$\tilde{u}_{1,I+1/2,J} = K^D_{1,I,J} \frac{D_{I,J}}{\triangle x_{I,J}}. \tag{41}$$

Next, we solve an analogous cell problem with boundary conditions B2 to find $K^D_{2,I,J}$. The two values $K^D_{1,I,J}, K^D_{2,I,J}$ form the diagonal upscaled tensor $\mathbf{K}^D_{I,J}$. Repeating cell calculations on all cells I, J of the grid at scale H, we obtain the collection of diagonal conductivities $\mathbf{K}_H \equiv \left(\mathbf{K}^D_{I,J}\right)_{IJ}$.

Instead of using Dirichlet boundary conditions B1, B2, one can solve (37)–(40) subject to periodic boundary conditions (34), (35), see BP in Figure 4. The jump is now D_{IJ}. However, the coefficients $(\mathbf{K}_H)^P_{IJ}$ that one gets from inverse matching of fluxes across all boundaries are, in general, not diagonal even if $\mathbf{K}_h$ is diagonal.

The global system $-\nabla_H \cdot (\mathbf{K}_H \nabla_H p_H) = 0$ solved for p_H on grid H with $(\mathbf{K})^M_H$ for $M = D, P$, has reasonable accuracy of global flow patterns in the sense that they resemble closely those for grid h. In general, $M = P$ leads to better accuracy of global flow patterns than $M = D$ does, and both are more accurate than $M = A, \mathcal{H}$. See further discussion of metrics of upscaling accuracy in Section 5.

4.2 Upscaling non-Darcy flow with a pressure-based method

For non-Darcy flow, the underlying problem at scale h is nonlinear and therefore it is not straighforward to see whether the problem at scale H has the same structure as the one at scale h, and even if so, how to obtain $\mathbf{K}_h \mapsto \mathbf{K}_H$, and $\beta_h \mapsto \beta_H$.

The following idea comes to mind. Let us be given $\mathbf{K}_h, \beta_h$ and some scale $H >> h$. Let $M = D$, hence, we focus for the moment on a pressure-based method using Dirichlet boundary conditions. Consider Ω_{IJ} and compute solutions to the cell problem on Ω_{IJ} similar to (37) first setting $\beta_h \equiv 0$ (Darcy case). Next, we compute the solution with β_h as was given originally. In each cell $\Omega_{I,J}$, the former gives us $\mathbf{K}^D_{IJ}$ while the latter can be used to find a nonlinear transmissibility $\Upsilon^{D,\mathcal{V}}_{IJ}$. Then find the upscaled β^D_{IJ} by fitting the nonlinear transmissibility, $\mathbf{K}^D_{IJ}$, D_{IJ} and the fluxes to the analogue of (20); see details in Section 4.2.1.

This procedure appears quite straightforward. However, the transmissibilities in non-Darcy flow depend nonlinearly on the fluxes, hence, β^D_{IJ} depends on the boundary conditions D_{IJ} driving the flow. In other words, β_H is not in general constant, but rather a function of gradients of pressure. When used in the global model (36), β_H will be chosen depending on p_H, or $\mathbf{u}_H$.

Therefore, the proposed procedure is only useful as a method of upscaling if i) β_H satisfies the same qualitative properties that β_h does, and if ii) we are able to determine *how it changes* quantitatively with the boundary conditions. In particular, i) β_H should be positive. As concerns ii), since Darcy's law and its discrete counterparts are linear, the coefficient $\mathbf{K}^D_{I,J}$ does not depend on $\alpha = D_{IJ}$. However, the fluxes do, and therefore the transmissibilities $\Upsilon^{D,\mathcal{V}}_{IJ}$ and hence β^D_{IJ} also are functions of α.

Beside qualitative guesses, we found it impossible to predict the character of the map $\beta_H(\alpha)$ analytically. It has to be computed numerically but is found to vary only midly; see Section 5.2. In general, only simple smooth relationships appear useful in

practice, so that it is enough to determine $\beta_H(\alpha)$ on a small set $\alpha \in A$: the values for $\alpha \in \mathbb{R}$ can be found via appropriate interpolation or approximation.

4.2.1 Details of upscaling $\beta_h \mapsto \beta_H$

Now we supply details of the method. Fix I, J. Consider variant $\mathcal{V} = 0$ or $\mathcal{V} = 1$. Find $\mathbf{K}^D_{IJ}$ by solving (37)–(40). Next, consider the following extension of (37)–(40) to non-Darcy flow

$$-\nabla_h \cdot \left(\mathbf{T}^{\mathcal{V}}_h \nabla_h \hat{p}_h\right) = 0, \quad \mathbf{y} \in \Omega_{IJ} \tag{42}$$

$$\hat{p}|_{\Gamma_{1,I-1/2,J}} = 0 \tag{43}$$

$$\hat{p}|_{\Gamma_{1,I+1/2,J}} = D_{I,J} \tag{44}$$

$$(\mathcal{T}(\nabla_h \hat{p}_h) \cdot \mathbf{n})|_{\Gamma_{2,I,J+1/2} \cup \Gamma_{2,I,J-1/2}} = 0. \tag{45}$$

This cell problem is solved with the numerical method and Newtonian iteration described in Sections 3 and 7.1.

Once $\hat{p}_h, \hat{u}_h$ are known, compute the total flux $\hat{u}_{1,I+1/2,J} = \int_{\Gamma_{1,I,J+1/2}} \hat{u}_h \cdot \mathbf{n}$, and find the value $\Upsilon^D_{1,I,J}$ from (20)

$$\hat{u}_{1,I+1/2,J} = \Upsilon^D_{1,I,J} \frac{D_{I,J}}{\triangle x_{I,J}}. \tag{46}$$

Finally, compute $\beta^D_{1,IJ}$ from (20)

$$\beta^D_{1,IJ} = \frac{\left(\Upsilon^D_{1,I,J}\right)^{-1} - (K^D_{1,IJ})^{-1}}{|\hat{u}_{1,I+1/2,J}|}. \tag{47}$$

Analogous calculations are done for $\beta_{2,IJ}$.

Collecting $\Upsilon^D_{1,IJ}, \Upsilon^D_{2,IJ}$ for all cells (I, J) we have Υ^D_H. By collecting $\beta^D_{1,IJ}, \beta^D_{2,IJ}$ computed componentwise, we finally obtain β^D_H.

Consider now $M = P$. It is straightforward to extend the above procedure to the case of periodic boundary conditions for cell problems; we have done this computationally. However, the process results in nondiagonal $\mathbf{K}^P_H, \Upsilon^P_H$ and in more than two components of β^P_{IJ}. The resulting upscaled model for the full matrix β^P_H lacks a theoretical foundation, and we defer it to future investigation.

4.3 Other methods of upscaling β_h

Consider now $M = A, \mathcal{H}$ and simple averaging procedures which yield $K^A_H, K^{\mathcal{H}}_H$.

Consider some divergence-free velocity field ψ_h on Ω_{ij} chosen ad-hoc, that is, without the pressure-solve of (42)–(45). For example, consider ψ_h arising as a gradient of linear pressure field satisfying (43)–(44), that is, a uniform velocity field. Note that since ψ_h is constant, trivially $\nabla_h \cdot \psi_h = 0$. Another possibility is to use as ψ_h the Darcy velocities found in (41). In each case ψ_h depends linearly on D_{IJ}. Now one can calculate a fixed quantity $\Upsilon(\mathbf{K}_h, \beta_h, \psi_h)$ which is "like" a transmissibility but which is inconsistent with (20). Putting aside the concern of inconsistency, a simple average Υ^M_{IJ} of $\Upsilon(\mathbf{K}_h, \beta_h, \psi_h)$ for $M = A, \mathcal{H}$ can be computed. Following a calculation similar

to (47) one obtains β_H^M for $M = A, \mathcal{H}$. This method of upscaling is very inexpensive computationally, and may offer advantages in some cases especially in layered media. For lack of space we do not present results.

5 Results

Here we illustrate results of the upscaling methodology proposed in Section 4 and we verify its accuracy; this follows in Sections 5.2 and 5.3. For the sake of exposition we provide first an illustration of numerical methods and effects of heterogeneity for non-Darcy flow (Section 5.1).

5.1 Non-Darcy flow results

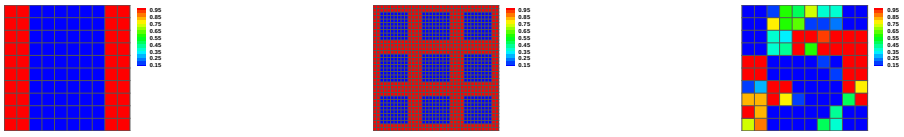

a) b) c)

Fig. 5 Field $\mathbf{K}_h$ for three cases a) layered, b) periodic (jump of a factor of 10), c) heterogeneous

Consider a 2D region of flow with $\mathbf{K}_h$ as shown in Figure 5 with permeability field a) layered isotropic, b) periodic (similar to a fracture system), and c) small heterogeneous. For each $\mathbf{K}_h$, let β_h be given by (6) with $\mathcal{B} = 0, 1$, and β_0 as indicated in each case. Now solve the problem (53) subject to boundary conditions of type B1, B2, or B3, as shown in Figure 4, with unit Dirichlet data. In the numerical model we consider velocity variants $\mathcal{V} = 0, 1$ as in (26). Below follows a discussion of most interesting and at the same time simple enough cases.

As concerns the layered case a), the results shown earlier in Section 2.1 in Figure 2 c) are representative of cross-sections when $\mathbf{K}_h$ is layered and boundary conditions B1 are used. With large β_0, the profiles of pressure become more typical of those for a homogeneous medium. If boundary conditions B2 are used, the flow field is uniform; we skip the presentation of these results.

Results for the periodic field b) are shown in Figure 6. Here, we use boundary conditions B3 in order to make the flow patterns interesting enough. The same effect of smoothing effects of larger β_0 on pressure profiles is observed.

Next we show the effects of the choice of $\mathcal{B}$ and of $\mathcal{V}$; we focus on the heterogeneous case c) and use $\beta_0 = 100$. See Figure 8, where pressure profiles for different choices of $\mathcal{B}, \mathcal{V}$ are shown. It is evident that the solutions for different variants $\mathcal{V} = 0, 1$ do not differ much; this is also true for other values of β_0 (not shown). However, as expected, the solutions for different $\mathcal{B} = 0, 1$ differ substantially. This suggests that care must be taken in real simulations to determine an appropriate model (6) of β.

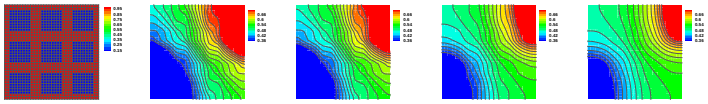

Fig. 6 Heterogeneity effects for non-Darcy flow, boundary condition B3, permeability field periodic, and $\mathcal{B} = 0, \mathcal{V} = 0$. Far left: reference field $\mathbf{K}_h$. Left to right: pressure profiles p_h for $\beta_0 = 0$ (Darcy), $\beta_0 = 1, 10^2, 10^3$, respectively.

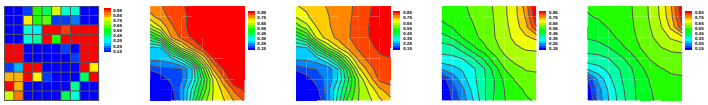

Fig. 7 Heterogeneity effects for non-Darcy flow, boundary condition B3, permeability field heterogeneous, and $\mathcal{B} = 0, \mathcal{V} = 0$. Far left: reference field $\mathbf{K}_h$. Left to right: pressure profiles p_h for $\beta_0 = 0$ (Darcy), $\beta_0 = 1, 10^2, 10^3$, respectively.

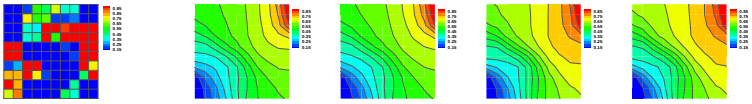

$\mathcal{B} = 0, \mathcal{V} = 0$ $\mathcal{B} = 0, \mathcal{V} = 1$ $\mathcal{B} = 1, \mathcal{V} = 0$ $\mathcal{B} = 1, \mathcal{V} = 1$

Fig. 8 Dependence of numerical solution on the choice of $\mathcal{B}, \mathcal{V}$. In all examples we use $\beta = 100$.

5.2 Results of upscaling

Now we come to the central issue of this paper on upscaling $\mathbf{K}_h, \beta_h$. Given $\mathbf{K}_h, \beta_h$ we want to i) compute $\mathbf{K}_H, \beta_H$, ii) use these to solve for p_H, and iii) verify the accuracy of our upscaling procedure. Throughout this section we use $H = Nh$ with $N > 1$.

We restrict presentation to the method $M = D$ using pressure-based solver with Dirichlet boundary conditions; as mentioned above, $M = P$ leads to still open theoretical questions on the form of non-Darcy correction. Methods $M = A, \mathcal{H}$ are very simple but in general less accurate than $M = D, P$ due to inconsistency and will not be discussed.

For logical verification of the upscaling methodology we first set up a trivial problem with $\mathbf{K}_h \equiv const = \mathbf{K}_0$, with some given isotropic or anisotropic $\mathbf{K}_0$. Clearly we obtain $\mathbf{K}_H = \mathbf{K}_0$ for any H. One can also expect that for any β_0 and $\beta_h = g_{\mathcal{B}}(\beta_0, \mathbf{K}_h)$, our upscaling procedure should deliver $\beta_H = g_{\mathcal{B}}(\beta_0, \mathbf{K}_H)$. This expectation is readily confirmed by numerical results for all cases $\mathcal{B} = 0, 1,\ \mathcal{V} = 0, 1$; detailed presentation is omitted.

Next we consider nontrivial $\mathbf{K}_h$. We compute $\mathbf{K}_H$ (upscaled Darcy permeability) for $\mathbf{K}_h, H$ as indicated in Figure 9. We then let $\beta_h = g_{\mathcal{B}}(\beta_0, \mathbf{K}_h)$, consider $\mathcal{B} = 0, 1$ and $\mathcal{V} = 0, 1$ and use the upscaling procedure defined in Section 4 with Dirichlet boundary data $p_D = \alpha$ which is allowed to vary and thus determine $\beta_H(\alpha)$. The collection of values α in practice need not be large.

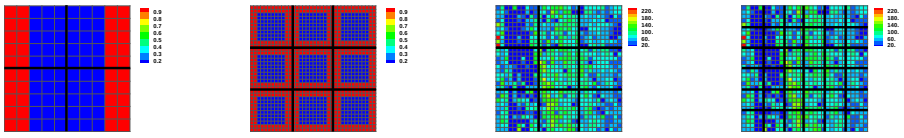

Fig. 9 Field $\mathbf{K}_h$ and grid H indicated by thick grid lines for three cases a) layered, b) periodic, c) large heterogeneous with 3x3 coarse grid, d) large heterogeneous with 6x6 coarse grid

Of interest is variability of β_H on Dirichlet boundary data α, and its anisotropy, particularly when β_h itself is isotropic. In general, we find nonisotropic β_H even if β_h is isotropic, and that $\beta_H \neq g(\beta_0, \mathbf{K}_H)$.

In the case of constant β_h we find

$$\begin{aligned} \mathcal{B} = 0 : \beta_h &= g_0(\beta_0, K_h) \equiv \beta_0 \\ \beta_H(\alpha) &= \big(\beta_{H,1}(\alpha), \beta_{H,2}(\alpha)\big) = (\mathcal{R}_1(\alpha), \mathcal{R}_2(\alpha))\, \beta_0, \end{aligned} \tag{48}$$

where both ratios $\mathcal{R}_x, \mathcal{R}_y$, for a fixed β_0, are mildly varying functions of α.

In the correlated case we find, abusing notation as concerns diagonal components of $\mathbf{K}_h$ and $\mathbf{K}_H$,

$$\begin{aligned} \mathcal{B} = 1 : \beta_h &= g_1(\beta_0, \mathbf{K}_h) = \frac{\beta_0}{\sqrt{K_h}}, \\ \beta_H(\alpha) &= \big(\beta_{H,1}(\alpha), \beta_{H,2}(\alpha)\big) = \frac{(\mathcal{R}_1(\alpha), \mathcal{R}_2(\alpha))\, \beta_0}{\sqrt{K_H}}. \end{aligned} \tag{49}$$

Remark 1 In summary, we find that

$$\beta_H(\alpha) = g_{\mathcal{B}}(\beta_0, \mathbf{K}_H)\, (\mathcal{R}_1(\alpha), \mathcal{R}_2(\alpha))\,, \tag{50}$$

that is, β_H is constant or correlated to $\mathbf{K}_H$, up to a non-isotropic multiplicative correction dependent on α.

The usefullness of our upscaling procedure depends on the range and variability of $\mathcal{R}_i(\alpha), i = 1, \ldots d$. In particular, in order for non-Darcy flow to retain its physical character reflected by monotonicity of the map $\mathcal{K}(K, \beta; D)$, we expect that each of the ratios must be positive; this is confirmed in our experiments. Results depend on $\mathbf{K}_h, \mathcal{B}$ and less significantly on $\mathcal{V}$, see below. Finally, the variability of $\mathcal{R}_i(\alpha), i = 1, \ldots d$ turns out to be small and so our upscaling method in practice does not require tremendous computational effort: $\mathcal{R}_i(\alpha), i = 1, \ldots d$ needs to be computed only for a few values of α.

5.2.1 Upscaled map β_H for layered case

First we discuss the results of the layered case, as they are quite illuminating; see Figure 10. If $\mathcal{B} = 0$ and $\beta_h \equiv \beta_0$, it is at a first glance reasonable to expect that the upscaled $\beta_H = g_{\mathcal{B}}(\mathbf{K}_H) \equiv \beta_0$. However, this is in fact only true for the flow *across* the layers, where we see that$\mathcal{R}_1(\alpha) \equiv 1$. We hypothetise that this is due to harmonic weighting of transmissibilities which is in perfect agreement with arithmetic averaging

of β_h and a constant unidirectional flux. On the other hand, the $\mathcal{R}_2(\alpha)$ is not constant and it is decreasing with α. In summary, in this case we obtain

$$\beta_H(\alpha) = (1, \mathcal{R}_2(\alpha))\beta_0. \tag{51}$$

However, we find that while β_H does indeed vary with both α and β_0, the ratios $\mathcal{R}_i$ remain mildly varying as functions of the product of $\beta_0\alpha$. Qualitatively, this is not surprising given the analytical solution derived in Section 2.1, see also Figure 2. From computational point of view, this property makes our upscaling method effective because results obtained for a fixed β_0 and several values of α can be reused for another set of values of β_0 and α.

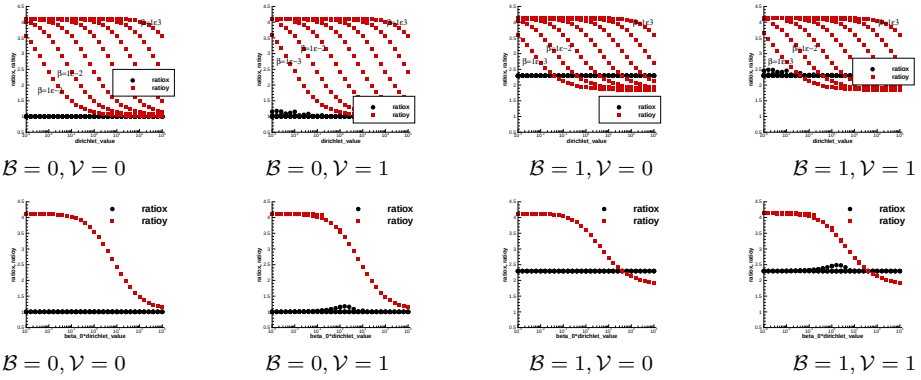

$\mathcal{B} = 0, \mathcal{V} = 0$ $\mathcal{B} = 0, \mathcal{V} = 1$ $\mathcal{B} = 1, \mathcal{V} = 0$ $\mathcal{B} = 1, \mathcal{V} = 1$

$\mathcal{B} = 0, \mathcal{V} = 0$ $\mathcal{B} = 0, \mathcal{V} = 1$ $\mathcal{B} = 1, \mathcal{V} = 0$ $\mathcal{B} = 1, \mathcal{V} = 1$

Fig. 10 Upscaled map $\beta_H(\alpha)$ for the layered case. Each figure shows $\mathcal{R}_1(\alpha), \mathcal{R}_2(\alpha)$ called 'ratiox,ratioy', respectively, for various values of β_0. Top: dependence of $\mathcal{R}_i(\alpha)$. Bottom shows $\mathcal{R}_i$ as a function of the product $\alpha\beta_0$.

5.2.2 Upscaled map β_H for heterogeneous case

Observations similar to the layered case can be made for the periodic and heterogeneous cases, where $\mathbf{K}_h$ is as in Figure 9b) and c). Of these two, the heterogeneous case is more interesting; see results shown in Figure 11. (We show only $(\beta_H)_{11}(\alpha)$).

The main observation with respect to the layered case is that both $\mathcal{R}_i, i = 1, 2$ vary with α and β_0. This obviously results from nonuniform flow in both $x_i, i = 1, \ldots d$ directions.

5.3 Comparison of fine and coarse grid solutions

Now we discuss the accuracy of upscaling non-Darcy flow by comparing results on coarse grid H to those on the original fine grid h.

In various papers devoted to upscaling, authors use different metrics to compare fine grid and coarse grid solutions; some compare p_h and p_H pointwise, some only show profiles of pressures and/or discuss agreement of velocity and streamline patterns between the two grids. In other papers, when wells are included, the well rates are

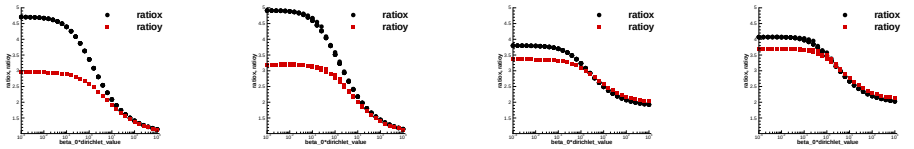

$\mathcal{B}=0,\mathcal{V}=0$ $\mathcal{B}=0,\mathcal{V}=1$ $\mathcal{B}=1,\mathcal{V}=0$ $\mathcal{B}=1,\mathcal{V}=1$

Fig. 11 Upscaled map $\beta_H(\alpha)$ for heterogeneous case when $\beta_h = g_{\mathcal{B}}(\beta_0, \mathbf{K}_h)$. Each figure shows $(\mathcal{R}_1, \mathcal{R}_2)$ denoted by ratiox, ratioy, respectively, as a function of the product $\alpha\beta_0$.

compared. On the other hand, it was pointed out that minimizing a particular norm of $p_h - p_H$ may be associated with a particular upscaling method, see [28,49]. In general, conclusions of comparisons depend on the metric that was chosen, and on the global boundary conditions and/or flow patterns. Finally, one should consider both accuracy and efficiency of an unpscaling method.

In this paper we compare boundary fluxes across outflow parts of $\partial\Omega$

$$f = \int_{\Gamma_{outflow}} \mathbf{K}\nabla p \cdot \nu,$$

and we also consider the following.

Remark 2 In any comparison one has to keep in mind the fact that, due to numerical error arising from discretization on grid h or H, the difference between solutions on grid h and H, regardless of the metrics, will likely be non-zero *even for homogeneous uniform* $\mathbf{K}_h$. (This does not apply directly to mortar or subgrid upscaling; see [42,38, 2]). To alleviate the effect of discretization error on upscaling error, one can compare the solution p_h on grid h obtained using $\mathbf{K}_h, \beta_h$, to that $p_{H\mapsto h}$ computed on the same grid h but with data $\mathbf{K}_{H\mapsto h}, \beta_{H\mapsto h}$. Here by $\mathbf{K}_{H\mapsto h}, \beta_{H\mapsto h}$, we mean $\mathbf{K}_H, \beta_H$ which were *downscaled* to the original grid h, for example by simple injection. We found this method of comparison very useful, but it requires computation of a solution $p_{H\mapsto h}$ on grid h which is expensive and does not relate directly to p_H. We emphasize that this idea is suggested only for theoretical purposes to compare various upscaling methods M; in a practical upscaling simulation it would not be employed. See Table 1 for comparison of four upscaling methods $M = A, D, P, \mathcal{H}$ for Darcy case for all three types of boundary conditions B1, B2, and B3, for heterogeneous $\mathbf{K}_h$.

Now we discuss results for non-Darcy upscaling; we test the accuracy of nonlinear upscaling relative to the accuracy of upscaling the linear Darcy case. We consider various patterns of $\mathbf{K}_h$ and H, shown in Figure 9. As before, β_h, is given by (6). We consider three cases of global boundary conditions B1, B2, and B3 as in Figure 4 so that the flow is from right to left, top to bottom, or crossflow from right to left, respectively. We use a prescribed global gradient of pressure D and fix $\mathcal{B}, \mathcal{V}$.

We first compute $\mathbf{K}_H$ and the map β_H for each case, as shown in Section 5.2. To verify that it is important to *calculate* the upscaled map β_H via (48)–(49) rather than to use the original value or correlation, we also set

$$\beta_H^g(\alpha) = g(\beta_0; \mathbf{K}_H). \tag{52}$$

Then we solve for p_h on grid h and for p_H and p_H^g on grid H, and compute fluxes.

Table 1 Comparison of $M = A, D, P, \mathcal{H}$ for Darcy flow for heterogeneous $\mathbf{K}_h$. Note that flux f_H for $M = A$ / $M = \mathcal{H}$ seems to always overpredict/ underpredict f_h; this is consistent with Hashin-Shtrikman bounds [29,45]. Also, $M = D, P$ give significantly more accurate results than $M = A, \mathcal{H}$. Note that $M = P$ while in general more accurate than $M = D$ here may be less so due to the off-diagonal terms of $\mathbf{K}_H^P$ which are dropped. Finally, for more complicated flow pattern associated with B3, the use of downscaled solution shows that the coefficients $\mathbf{K}_H$ and the numerical error are jointly contributing to (in)accuracy of upscaled solution.

BC	M	f_h	f_H	$f_{H\mapsto h}$	$\lvert\frac{f_h-f_H}{f_h}\rvert$	$\lvert\frac{f_h-f_{H\mapsto h}}{f_h}\rvert$
B1	A	32.57484362	55.03545873	55.09824639	0.68950799	0.69143548
	D	32.57484362	32.35069719	32.38584459	0.00688097	0.00580199
	P	32.57484362	32.41986422	32.45464733	0.00475764	0.00368985
	$\mathcal{H}$	32.57484362	26.14566346	26.17359339	0.19736642	0.19650901
B2	A	51.38471961	58.92646422	58.97261428	0.14677018	0.14766831
	D	51.38471961	51.34424224	51.38080698	0.00078773	0.00007614
	P	51.38471961	50.55448835	50.58589065	0.01615716	0.01554604
	$\mathcal{H}$	51.38471961	35.73207110	35.77021427	0.30461679	0.30387449
B3	A	17.85362214	20.76764487	26.32567940	0.16321745	0.47452876
	D	17.85362214	13.98183753	17.75764287	0.21686269	0.00537590
	P	17.85362214	13.85705590	17.63303101	0.22385184	0.01235554
	$\mathcal{H}$	17.85362214	10.29882863	12.91371346	0.42315186	0.27668944

Table 2 Layered case upscaled to 2x2. Column BC describes the boundary condition used.

BC	D	β_0	f_h	f_H	$\lvert\frac{f_h-f_H}{f_h}\rvert$	f_H^g	$\lvert\frac{f_h-f_H^g}{f_h}\rvert$
B1	1	0	0.15625	0.156250	0	0.156250	0
B2	1	0	0.46	0.460000	1.2e-016	0.460000	1.2e-016
B1	1	0.01	0.156212	0.156212	1.4e-013	0.156212	1.4e-013
	1	1	0.152611	0.152611	2.9e-015	0.152611	2.9e-015
	1	100	0.072995	0.072995	1.9e-016	0.072995	1.9e-016
	100	1	7.29952	7.299524	2.4e-016	7.299524	2.4e-016
	0.01	1	0.001562	0.001562	1.4e-013	0.001562	1.4e-013

Remark 3 To compute p_H, one needs to use the upscaled map $\beta_H(\alpha)$, that is, we have to select the particular α that is needed. The α can be found by iteration lagging in global Newton iteration described in Section 7.1. Since $\beta_H(\alpha)$ does not have large derivatives, such estimation does not introduce much additional error.

Results corresponding to permeability cases from Figure 9 are summarized in Tables 2, 3, 4, respectively. Additionally, pressure profiles are shown for selected examples. Discussion follows. For the sake of brevity as before we restrict ourselves to only most interesting cases and results. Recall also that non-Darcy case results are only considered for $M = D$ for reasons explained above. We do not show downscaled results for lack of space; they are qualitatively consistent with non-downscaled results.

5.3.1 Upscaling of layered case

In the layered case and B1 and B2, the agreement of f_h and f_H is perfect. This is expected: for B1, the upscaled value $\mathbf{K}_H$ agrees with harmonic average, and for B2 with arithmetic average of $\mathbf{K}_h$, and this is reflected in the values of f_h, f_H for Darcy case $\beta = 0$. For $\beta \neq 0$, we have that β_H is constant and so $p_H = p_H^g$ and we see also very good agreement of f_h with both f_H, f_H^g. Other results for B1, B2 reproduce the same behavior.

Table 3 Results of non-Darcy upscaling for periodic case upscaled to 3x3 grid. Here we show results for B1 only, since the case is symmetric.

D	β_0	f_h	f_H	$\lvert\frac{f_h-f_H}{f_h}\rvert$	f_H^g	$\lvert\frac{f_h-f_H^g}{f_h}\rvert$
1	0	0.451148	0.451148	8.06e-007	0.451148	8.06e-007
		$\mathcal{V}=0,\mathcal{B}=0$				
	0.01	0.44762	0.447621	7.77e-007	0.450233	0.00583
	0.1	0.420943	0.420943	5.70e-007	0.442321	0.050787
	1	0.312592	0.312592	5.31e-008	0.384463	0.22992
	10	0.174966	0.174966	5.43e-007	0.224258	0.28172
	100	0.079319	0.079319	8.33e-007	0.089529	0.12872
1	0	0.451148	0.451148	8.06e-007	0.451148	8.1e-07
0.01	1	0.004473	0.004476	1.46e-005	0.004502	0.00594
0.1	1	0.042045	0.042050	0.000116	0.044232	0.05200
1	1	0.311185	0.311187	6.23e-006	0.384463	0.23547
10	1	1.74129	1.741323	2.04e-005	2.242580	0.28788
100	1	7.92272	7.922750	4.41e-006	8.952939	0.13003
		$\mathcal{V}=0,\mathcal{B}=1$				
1	0	0.451148	0.451148	8.06e-007	0.451148	8.06e-007
1	0.01	0.447594	0.447595	7.77e-007	0.449789	0.00490
1	1	0.310331	0.310331	6.72e-008	0.362759	0.16894
1	100	0.0671734	0.067173	9.04e-007	0.074849	0.11426
		$\mathcal{V}=1,\mathcal{B}=0$				
1	0	0.451148	0.451148	8.06e-007	0.451148	8.06e-07
	0.01	0.447573	0.447561	2.55e-005	0.450233	0.00594
	0.1	0.420478	0.420481	7.89e-006	0.442321	0.05194
	1	0.311185	0.311187	6.24e-006	0.384463	0.23547
	10	0.174126	0.174132	3.35e-005	0.224257	0.28790
	100	0.0792157	0.079227	0.000149	0.089529	0.13019

5.3.2 Upscaling periodic case

In the periodic case, if β_H is used, the upscaled fluxes f_H are as accurate as in the layered case for all cases with $\mathcal{B}=0,1$ and $\mathcal{V}=0,1$. However, the fluxes f_H^g are not in very good agreement with f_h. See Table 3.

5.3.3 Upscaling heterogeneous case

We consider isotropic and anisotropic variants. In the latter case, $(K_2)_{ij}=5(K_1)_{ij}$. Results are, respectively, in Table 4, and in Table 5. It can be seen from Table 4 that the use of β_H gives significantly better results than the use of β_H^g. In particular, when comparing the results for $\beta=0$ to those for $\beta\neq 0$, we see that the fluxes f_H are, at least for B1 and B2, quite close to f_h. In the non-isotropic case the results of non-Darcy upscaling appear in better agreement than those with Darcy case.

5.3.4 Correlation between β_H and $\mathbf{K}_H$

Our last result answers a natural question, and let $\mathcal{B}=0$ and $\beta_0=1$. Let us be given a fine grid heterogeneous $\mathbf{K}_h$ such as in Figure 9, c). After $\mathbf{K}_H$ and $\beta_H(\alpha)$ are computed, the questions is: for a fixed α, is there any correlation between $\beta_H(\alpha)$ and $\mathbf{K}_H$?

The answer is illustrated in Figure 15 and it appears to suggest a mild correlation $\beta_H\approx c(\mathbf{K}_H)^s$ where $s<0$ and $|s|$ is small, and which is qualitatively independent of β_0 or α.

Table 4 Results for heterogeneous, isotropic case. Upscaling to 3x3 and 6x6; only interesting cases shown. Throughout $\mathcal{V} = 0$.

BC	D	β_0	f_h	f_H	$\lvert\frac{f_h - f_H}{f_h}\rvert$	f_H^g	$\lvert\frac{f_h - f_H^g}{f_h}\rvert$
B1	1	0	32.5748	32.350697	0.0068809674	32.350697	0.00688
B2	1	0	51.3847	51.344242	0.00078773182	51.344242	0.00078773182
B3	1	0	17.8536	13.981838	0.21686269	13.981838	0.21686269
	$\mathcal{B} = 0$ **upscaling to 3x3**						
B1	1	0.01	8.30372	8.292560	0.0013440962	8.535338	0.02789
	1	1	0.98079	0.980768	2.26e-005	0.984167	0.0034434907
	1	100	0.0998039	0.099805	9.14e-006	0.099840	0.00036680035
B1	0.01	1	0.0830359	0.082925	0.0013346016	0.085353	0.027909566
	1	1	0.98079	0.980768	2.26e-005	0.984167	0.0034434907
	100	1	9.98054	9.980541	8.34e-009	9.984043	0.0003509255
	$\mathcal{B} = 1$ **upscaling to 3x3**						
B1	1	0.01	16.4825	16.581159	0.0059877337	16.736875	0.015435089
	1	10	0.771172	0.788014	0.021839215	0.758147	0.016889485
	1	1	2.36765	2.416472	0.020619331	2.335706	0.013492875
	1	100	0.246165	0.251634	0.022216664	0.241736	0.017991781
	10	1	7.71176	7.880148	0.0218355	7.581472	0.016894391
B2	1	0.01	8.46364	8.392461	0.0084098349	8.980445	0.061061964
	1	1	0.981007	0.980862	0.00014691914	0.989225	0.0083772249
	1	100	0.0998052	0.099805	4.8381498e-006	0.099892	0.00086514693
	$\mathcal{B} = 0$ **upscaling to 3x3**						
B3	1	1	0.537621	0.443146	0.17572764	0.445521	0.17131009
	1	0.01	4.49917	3.685097	0.18093908	3.846547	0.14505487
	1	100	0.0548129	0.045192	0.17552435	0.045217	0.17507379
	$\mathcal{B} = 1$ **upscaling to 3x3**						
B3	1	0.01	8.90008	7.152788	0.19632361	7.416759	0.16666418
	1	1	1.28143	1.047498	0.18255851	1.043956	0.18532221
	1	100	0.133437	0.109215	0.18152499	0.108140	0.18958172
	$\mathcal{B} = 0$ **upscaling to 6x6**						
B1	1	0.01	8.30372	8.296412	0.00088023584	8.525850	0.0267505
	1	1	0.98079	0.980768	2.1964034e-005	0.984003	0.0032759738
	1	100	0.0998039	0.099804	2.4940728e-006	0.099838	0.00033819023
B2	1	0.01	8.46364	8.391858	0.0084810113	8.933469	0.055511652
	1	1	0.981007	0.980852	0.00015715651	0.988642	0.0077834603
	1	100	0.0998052	0.099805	1.6263878e-006	0.099885	0.00080476623

Table 5 Heterogeneous case 30x30 with anisotropy ratio 5 upscaled to 3x3. Throughout $\mathcal{B} = 0, \mathcal{V} = 0$.

BC	D	β_0	f_h	f_H	$\lvert\frac{f_h - f_H}{f_h}\rvert$	f_H^g	$\lvert\frac{f_h - f_H^g}{f_h}\rvert$
B1	1	0	34.8733	33.689881	0.033933817	33.689881	0.033933817
B2	1	0	243.981	246.780723	0.011473481	246.780723	0.011473481
B3	1	0	24.5257	18.026847	0.26498012	18.026847	0.26498012
B1	1	0.01	8.32665	8.305207	0.0025747009	8.586365	0.031191334
	1	1	0.980837	0.980788	4.967377e-005	0.984753	0.0039928307
	1	100	0.0998053	0.099805	3.2948047e-007	0.099846	0.00041092264
B2	1	0.01	9.63034	9.625004	0.00055404447	9.776467	0.015173625
	1	1	0.996125	0.996118	6.3406493e-06	0.997739	0.0016202148
	1	100	0.0999578	0.099934	0.00023912392	0.099977	0.00019552109
B3	1	0.01	4.71649	3.821925	0.18966706	3.988913	0.15426174
	1	1	0.540639	0.444926	0.1770378	0.447171	0.17288422
	1	100	0.0548442	0.045206	0.1757355	0.045233	0.17524023

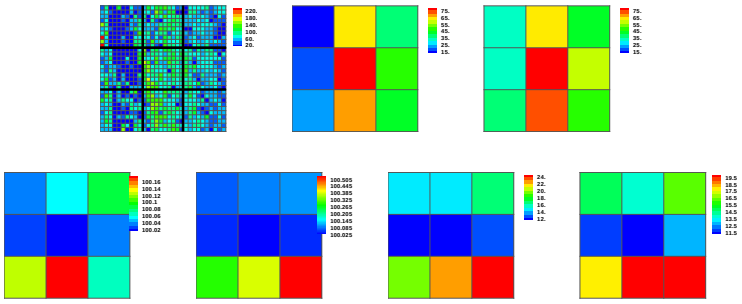

Fig. 12 Data for upscaling heterogeneous case to 3x3 grid. First row: original $\mathbf{K}_h$ (isotropic) and upscaled permeabilities $\mathbf{K}_H$ (nonisotropic). Second row: upscaled $\beta_{1,H}(1)$, $\beta_{2,H}(1)$ for $\beta_0 = 1e2$ for $\mathcal{B} = 0$ (left) and $\mathcal{B} = 1$ (right).

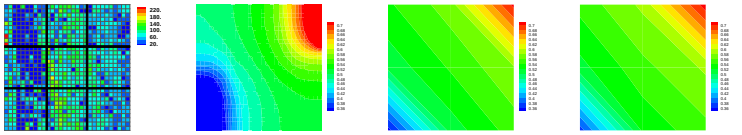

Fig. 13 Upscaling heterogeneous case to 3x3 grid with B3 boundary conditions: pressure contours for $\beta_0 = 100$, $\mathcal{B} = 0$. Far left: $\mathbf{K}_h$. Left: fine grid solution p_h, middle: p_H. Right: p_H^g.

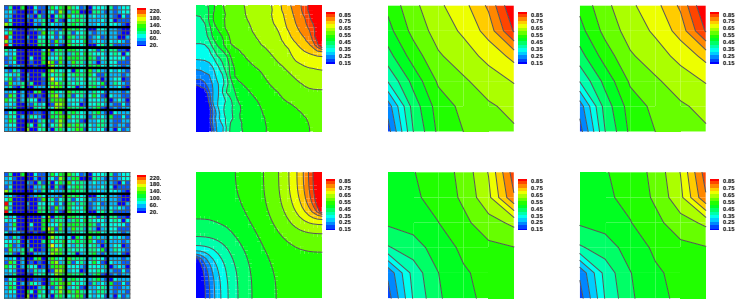

Fig. 14 Upscaling heterogeneous case to 6x6 grid with B3 boundary conditions: pressure contours for $\beta_0 = 0$ (top), and $\beta_0 = 1$. Throughout $\mathcal{B} = 0$. Far left: $\mathbf{K}_h$ and H. Left: fine grid solution p_h, middle: p_H. Right: p_H^g.

This *may* indicate why several authors report on *different* correlations between measured $\mathbf{K}$ and β; our calculations show that the computational correlations appear to depend on the scale at which they are measured.

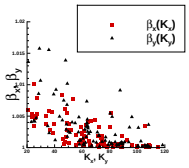

Fig. 15 Scatter-plot of $\beta_H(\alpha)$ vs $\mathbf{K}_H$ for $\alpha = 1$ for heterogeneous case.

6 Conclusions

In this paper we have addressed the issue of upscaling non-Darcy flow driven by boundary conditions, where a simple quadratic model of velocity parametrized with a positive coefficient β and conductivity $\mathbf{K}$ extends the linear Darcy case. Given $\mathbf{K}_h, \beta_h$ at fine scale h, the approach is to determine $\mathbf{K}_H, \beta_H$. Our method extends the one for Darcy case [14]. The resulting upscaled coefficient β_H is a mildly varying map which supplies an anisotropic correction to the original coefficient from fine scale. We presented the numerical method, the upscaling procedure, and numerical results which demonstrate the accuracy of the method. Some simple variants of the procedure which may be less computationally cumbersome but are also less accurate have been also proposed. Values of β_H appear correlated to some function(s) of $\mathbf{K}_H$; this appears independent of the correlation at fine scale.

There remain open questions as concern an appropriate anistropic model of non-Darcy correction, other non-Darcy models, fracture systems, as well as upscaling around wells. These are topics of future work.

Acknowledgements We would like to acknowledge the help of John Osborne (Oregon State University) with some upscaling computations.

We thank Jill Reese for reference to [44] where we found additional reference [26] to the work on non-Darcy flow for layered media; we were not familiar with this work prior to submitting our paper. Interestingly, our results concerning upscaled β_H for layered media appear consistent with those in [26].

We would like to thank the anonymous referees whose remarks helped to improve the paper.

7 Appendix

7.1 Nonlinear solver

Here we discuss the solution of the nonlinear discrete system that arises from (22), some imposed boundary conditions, and the implicit relation (31). In summary, we solve for p_h the system

$$\nabla_h \cdot \mathbf{T}_h^{\mathcal{V}} \nabla p_h = 0. \tag{53}$$

This system of equations is nonlinear and, if $\mathcal{V} = 1$, it additionally requires a local internal iteration to resolve the local implicit relationships (29), (30). The latter is not required for $\mathcal{V} = 0$.

Consider first $\mathcal{V} = 0$. One can compute explicitly $\mathbf{u}_h = \mathbf{T}^0(p_h)$ pointwise from (31), if only p_h is known. Since p_h is, of course, unknown, we have to solve (53) by iteration.

As initial guess $p_h^{(0)}$ one can use the Darcy pressures which can be found by solving a linear counterpart of (53) setting $\beta = 0$. Or, for large β, additionally one may try the *method of continuity* in which one starts with $\beta = 0$ and then iterates, gradually increasing β to the desired magnitude, thereby obtaining a better initial guess.

It appears very natural to solve (53) using successive substitutions iterating on (31). Unfortunately, for small h and large heterogeneities, this simple iteration may have trouble converging and/or is very slow. The only reasonable alternative is to use Newton's method. We set it up as follows.

Given an initial guess $p_h^{(0)}$, iterate for $n = 0, 1, \ldots$ until convergence

$$\begin{aligned}
(*)\quad \text{compute } \mathbf{u}_h^{(n)} &= \mathbf{T}^{\mathcal{V}}\left(\mathbf{K}_h, \beta_h, |\mathbf{u}_h^{(n)}|, \mathbf{u}_h^{(n)}\right) \nabla_h p_h^{(n)} \\
\text{compute residual } \mathbf{R}^{(n)} &= \nabla_h \cdot \mathbf{u}_h^{(n)} \\
\text{compute Jacobian } \mathbf{J}^{(n)} &= \frac{\partial}{\partial p_h} \mathbf{R}^{(n)} \\
\text{advance } p_h^{(n+1)} &= p_h^{(n)} - (\mathbf{J}^{(n)})^{-1} \mathbf{R}^{(n)}
\end{aligned}$$

In this algorithm, the step $(*)$ can be executed pointwise analytically, if $\mathcal{V} = 0$. The residual calculations of $\mathbf{R}^{(n)}$ are quite simple as we only have to calculate the current $\nabla_h \cdot \mathbf{u}_h^{(n)}$. Jacobian calculations of $\mathbf{J}^{(n)}$ are done with the help of (12). Overall however, the method converges generally quite fast, even for large β.

Consider now $\mathcal{V} = 1$. Now the step $(*)$ cannot be executed exactly and, in order to resolve (21), we compute an iteration-lagged approximation $\tilde{\mathbf{u}}_h^{(n)}$ to $\mathbf{u}_h^{(n)}$ via

$$\tilde{\mathbf{u}}_h^{(n)} = \mathbf{T}^{\mathcal{V}}\left(\mathbf{K}_h, \beta_h, |\mathbf{u}_h^{(n-1)}|, \tilde{\mathbf{u}}_h^{(n)}\right) \nabla_h p_h^{(n)}.$$

This introduces a mild inconsistency in the residual and Jacobian calculations. However, the Newton iteration converges at least as fast as the one for $\mathcal{V} = 0$. If the iteration is run under strict convergence tolerance criteria, then one can assume that $\tilde{\mathbf{u}}_h^{(n)} \approx \mathbf{u}_h^{(n)}$. Note that due to a different formulation $p_h, \mathbf{u}_h$ obtained with $\mathcal{V} = 0, 1$ are (somewhat) different, see results shown in Section 5.

Our experience with performance of the Newton solver for variants $\mathcal{V} = 0, 1$, models $\mathcal{B} = 0, 1$ of β_h and values of $\mathbf{K}_h$ can be summarized as follows. The solver needs more iterations in the case of strong anisotropy especially if β is correlated with $\mathbf{K}$. Next, one should formulate the stopping criteria very carefully: in terms of simple mass-balanced residual norms, the iteration appears not to be making much progress, while pressure and velocity values have not yet converged. As concerns velocity variants, variant $\mathcal{V} = 0$ requires more iterations to converge than $\mathcal{V} = 1$, especially for strong anisotropy ratio and large uncorrelated heterogeneities; this is likely caused by $\mathcal{V} = 1$ being capable of carrying more information. The opposite appears true for small correlation lengths, for example for the periodic fissure problem (see Section 5) and is probably due to the inconsistency of residuals discussed above playing more substantial role in the absence of other difficulties.

7.2 Mixed FE derivation of (25)

Here we use mixed finite elements of type $RT_{[0]}$ on a rectangular grid to derive (25); we focus on details leading to (26). Such derivation was done for Darcy's flow in [46].

The non-Darcy flow equations were discretized using mixed FE in [12,36] but, to our knowledge, the use of quadrature and identification with CCFD discussed here has not been carried out. The importance of this derivation is that it extends the convergence results of mixed FE to CCFD formulation; on the other hand, it uncouples the saddle point formulation of mixed FE [46]. For notation see also [6].

First consider the weak formulation of (1), (4) complemented by no-flow boundary conditions (33) with $\Gamma_N \equiv \partial\Omega$. Let $(W, \mathbf{V}) = (L^2(\Omega), \{\mathbf{v} \in H(div; \Omega) : \mathbf{v} \cdot \nu|_{\Gamma_N} = 0\})$. The weak solution $(p, \mathbf{u}) \in (W, \mathbf{V})$ satisfies the system obtained by by multiplying (4), (1) by test functions $w \in W, \mathbf{v} \in \mathbf{V}$ and integrating by parts over Ω

$$\int_\Omega \nabla \cdot \mathbf{u} w = \int_\Omega q w, \ \ \forall w \in W, \tag{54}$$

$$\int_\Omega \mathbf{K}^{-1}\mathbf{u} \cdot \mathbf{v} + \int_\Omega \beta|\mathbf{u}|\mathbf{u} \cdot \mathbf{v} = \int_\Omega p \nabla \cdot \mathbf{v}, \ \forall \mathbf{v} \in \mathbf{V} \tag{55}$$

The mixed FE solution $(p_h, \mathbf{u}_h) \in W_h \times \mathbf{V}_h$ where $W_h \subset W, \mathbf{V}_h \subset \mathbf{V}$. The functions in W_h are piecewise constant on each cell; a test function $\xi_{ij} \in W_h$ is a characteristic function of the cell $\Omega_{i,j}$ so that $p_h(x, y) = \sum_{ij} \xi_{ij}(x, y) p_{ij}$. Recall that the functions $\mathbf{v}_h \in \mathbf{V}_h$ from space $RT_{[0]}$ [43] are piecewise linear in one coordinate direction and piecewise constant in the others and can be written symbolically as a tensor product $RT_{[0]} = P_{1,0} \times P_{0,1}$ [6][46,43]. Here $P_{q,r}(S)$ denotes a space of polynomials of degree q in x_1 and of degree r in x_2 which are variables over a subset $S \subset \mathbb{R}^d$. We have

$$\begin{aligned}\mathbf{u}_h(x, y)|_{\Omega_{ij}} = \big(&\psi_{i-1/2,j}(x) u_{i-1/2,j} + \psi_{i+1/2,j}(x) u_{i+1/2,j} \ , \\ &\phi_{i,j-1/2}(y) v_{i,j-1/2} + \phi_{i,j+1/2}(y) v_{i,j+1/2}\big) \ ,\end{aligned}$$

with the basis functions $\psi_{i+/-1/2,j}(x), \phi_{i,j+/-1/2}(y)$ in $P_{1,0}$ and $P_{0,1}$, respectively. Note that $\psi_{i+1/2,j}(x)$ is supported only on $\Omega_{ij} \cup \Omega_{i+1,j}$.

It is also useful to consider the value of $\mathbf{u}_h$ on the edge $E_{i+1/2,j,k} = \partial\Omega_{ij} \cap \partial\Omega_{i+1,j}$. By definition of $\mathbf{u}_h$, we are guaranteed the continuity of its normal component $(\mathbf{u}_h)_1$ but not of its tangential component $(\mathbf{u}_h)_2$ across that edge. The discrete solution $(p_h, \mathbf{u}_h)$ satisfies an equation analogous to (54) in which

$$\int_\Omega \nabla \cdot \mathbf{u}_h w_h = \int_\Omega q w_h, \ \ \forall w_h \in W_h,$$

and using $w_h = \xi_{ij}$ one derives pointwise

$$u_{i+1/2,j} - u_{i-1/2,j} + u_{i,j+1/2} - u_{i,j-1/2} = q_{ij} \triangle x_i \triangle y_j, \tag{56}$$

which can be interpretted as (22) when $q \equiv 0$. The discrete analogue to momentum equation (55) is

$$\int_\Omega \mathbf{K}_h^{-1}\mathbf{u}_h \cdot \mathbf{v}_h + \int_\Omega \beta_h|\mathbf{u}_h|\mathbf{u}_h \cdot \mathbf{v}_h = \int_\Omega p_h \nabla \cdot \mathbf{v}_h, \ \ \forall \mathbf{v}_h \in \mathbf{V}_h \tag{57}$$

forming a linear saddle-point system along with (22).

Now, as shown in [46] for Darcy flow, the integrals in (57) can be replaced by their numerical approximations, namely, a combination of trapezoidal and midpoint quadrature rules, at the expense of introducing a quadrature error of higher order than approximation order. In this way the discrete velocity values are identified with those in

CCFD formulation; the numerical integration approach entirely decouples the original saddle-point system and allows to solve a symmetric non-negative-definite system in p_h unknown only. We notice that this is possible for diagonal $\mathbf{K}$.

We follow the same idea here for non-Darcy flow. Use the test function $\mathbf{v}_h = (\psi_{i+1/2,j}, \xi_{jk}) \in V_h$ and integrate over its support $\Omega_{ij} \cup \Omega_{i+1,j}$, with the trapezoidal rule applied to integration in x_1 direction and the midpoint rule applied in y_1 directions, which we denote by subscripts $_{(TM)}$.

The integration rules used below for products are all of second order accuracy with respect to the size of domain: trapezoidal $\left(\int_a^b f(t)g(t)dt\right)_T = (b-a)\frac{f(a)g(a)+f(b)g(b)}{2}$, the midpoint rule $\left(\int_a^b f(t)g(t)dt\right)_M = (b-a)f(\frac{a+b}{2})g(\frac{a+b}{2})$. Additionally, we define the product P rule as $\left(\int_a^b f(t)g(t)dt\right)_P = (b-a)f(\frac{a+b}{2})\frac{g(a)+g(b)}{2}$. One can show using standard numerical analysis that the P rule has (at least) the same order of accuracy as the trapezoidal rule.

Using the (TM) rule for the first integral on left hand side, and integrating directly the right hand side of (57) we obtain expressions as in Darcy's case, since $\mathbf{v}_h$ equals zero on both edges $E_{i-1/2,j}, E_{i+3/2,j}$

$$\begin{aligned}\left(\int_\Omega \mathbf{K}^{-1}\mathbf{u}_h \cdot \mathbf{v}_h\right)_{TM} &= \left(\int_{\Omega_{ij}} K_{1,ij}^{-1}\mathbf{u}_h \cdot \mathbf{v}_h\right)_{TM} + \left(\int_{\Omega_{i+1,j}} K_{1,i+1,j}^{-1}\mathbf{u}_h \cdot \mathbf{v}_h\right)_{TM} \\ &= \triangle y_j T_{1,i+1/2,j}^{-1} u_{i+1/2,jk}, \\ \int_\Omega p_h \nabla \cdot \mathbf{v}_h &= \int_{\Omega_{ij}} p_{ij}\nabla \cdot \mathbf{v}_h + \int_{\Omega_{i+1,j}} p_{i+1,j}\nabla \cdot \mathbf{v}_h = \triangle y_j (p_{ij} - p_{i+1,j}).\end{aligned}$$

The new and most important element in the non-Darcy case is handling of the second term on the left side of (57). Using the (TM) quadrature rule over $\Omega_{ij} \cup \Omega_{i+1,j}$, we get

$$\left(\int_\Omega \beta|\mathbf{u}_h|\mathbf{u}_h \cdot \mathbf{v}_h\right)_{TM} = \beta_{ij}\left(\int_{\Omega_{ij}} |\mathbf{u}_h|\mathbf{u}_h \cdot \mathbf{v}\right)_{TM} + \beta_{i+1,j}\left(\int_{\Omega_{i+1,j}} |\mathbf{u}_h|\mathbf{u} \cdot \mathbf{v}\right)_{TM} \quad (58)$$

Consider one of the integrals on the right side, which gives exactly

$$\left(\int_{\Omega_{ij}} |\mathbf{u}_h|\mathbf{u}_h \cdot \mathbf{v}\right)_{TM} = \frac{\triangle x_i \triangle y_j}{2}|(\mathbf{u}_h)_{ij}^+|u_{1,i+1/2,j}, \quad (59)$$

and which is consistent with $\mathcal{V} = 2$ in (26) and the following expression

$$\begin{aligned}\left(T_{1,i+1/2,j}^{-1} + \frac{1}{2}\left(\triangle x_i \beta_{1,ij}|\mathbf{u}_h|_{ij}^+ + \triangle x_{i+1}\beta_{1,i+1,j}|\mathbf{u}_h|_{i+1,j}^-\right)\right)u_{1,i+1/2,j} \quad (60)\\ = p_{i,j} - p_{i+1,j}.\end{aligned}$$

Since each $|\mathbf{u}_h|_{ij}^+, |\mathbf{u}_h|_{ij}^-$ depends on $u_{1,i+1/2,j}$ and on other velocity degress of freedom, as mentioned before, the solution $u_{1,i+1/2,j}$ cannot be obtained analytically or even by local iteration.

This issue can be somewhat rectified by the use, instead of the discontinuous values $|\mathbf{u}_h|^+_{ij}$, $|\mathbf{u}_h|^-_{ij}$ in (60), of their average $|\bar{\mathbf{u}}_h|_{ij}$ as in $\mathcal{V}=1$ leading to

$$\left(T^{-1}_{1,i+1,j}+\frac{1}{2}(\triangle x_i\beta_{1,ij}+\triangle x_{i+1}\beta_{1,i+1,j})|\frac{(\mathbf{u}_h)^+_{ij}+(\mathbf{u}_h)^-_{i+1,j}}{2}|\right)u_{1,i+1/2,j} = p_{i,j}-p_{i+1,j}. \quad (61)$$

This introduces an additional error which is however readily seen to be of order not exceeding that of numerical integration, via expansion, for any z, $\sqrt{1+z}=1+\frac{z}{2}-\frac{1}{8}z^2+O(z^3)$. Further details will not be provided as they are not essential.

Now we discuss $\mathcal{V}=3$. This arises if in (58) one uses the (PM) integration rule instead of (TM),

$$\left(\int_{\Omega_{ij}}|\mathbf{u}_h|\mathbf{u}_h\cdot\mathbf{v}\right)_{PM}=\frac{\triangle x_i\triangle y_j}{2}|(\mathbf{u}_h)_{ij}|u_{1,i+1/2,j}$$

which provides the following alternative to (27),

$$\left(T^{-1}_{1,i+1/2,j}+\frac{1}{2}\left(\triangle x_i\beta_{1,ij}|(\mathbf{u}_h)_{ij}|+\triangle x_{i+1}\beta_{1,i+1,j}|(\mathbf{u}_h)_{i+1,j}|\right)\right)u_{1,i+1/2,j} = p_{i,j}-p_{i+1,j}.$$

Since this formulation leads to an excessively wide stencil, it is not pursued here.

Finally we interpret $\mathcal{V}=0$. It arises if instead of (7) one discretizes (8). Alternatively, $\mathcal{V}=0$ can be seen as an approximation to $\mathcal{V}=1$ in which the tangential components of velocity are ignored.

References

1. Special issue devoted to upscaling in porous media. Computational Geosciences **6** (2002)
2. Arbogast, T.: An overview of subgrid upscaling for elliptic problems in mixed form. In: Current trends in scientific computing (Xi'an, 2002), *Contemp. Math.*, vol. 329, pp. 21–32. Amer. Math. Soc., Providence, RI (2003)
3. Barker, J., Thibeau, S.: A criticial review of the use of pseudo relative permeabilities for upscaling. SPE 35491 (1996)
4. Bear, J.: Dynamics of Fluids in Porous Media. Dover, New York (1972)
5. Bensoussan, A., Lions, J.L., Papanicolaou, G.: Asymptotic analysis for periodic structures, *Studies in Mathematics and its Applications*, vol. 5. North-Holland Publishing Co., Amsterdam (1978)
6. Brezzi, F., Fortin, M.: Mixed and hybrid finite element methods, *Springer Series in Computational Mathematics*, vol. 15. Springer-Verlag, New York (1991)
7. Chen, Y., Durlofsky, L.J.: Adaptive local-global upscaling for general flow scenarios in heterogeneous formations. Transport in Porous Media **62**(2), 157–185 (2006)
8. Chen, Y., Durlofsky, L.J., Gerritsen, M., Wen, X.H.: A coupled local global upscaling approach for simulating flow in highly heterogeneous formations. Adv. Water Resour **26**, 1041–1060 (2003)
9. Chen, Z.: Expanded mixed finite element methods for linear second-order elliptic problems. I. RAIRO Modél. Math. Anal. Numér. **32**(4), 479–499 (1998)
10. Chen, Z., Huan, G., Li, B.: A pseudo function approach in reservoir simulation. Int. J. Numer. Anal. Model. **2**(suppl.), 58–67 (2005)
11. Chen, Z., Yue, X.: Numerical homogenization of well singularities in the flow transport through heterogeneous porous media. Multiscale Model. Simul. **1**(2), 260–303 (electronic) (2003)

12. Douglas Jr., J., Paes-Leme, P.J., Giorgi, T.: Generalized Forchheimer flow in porous media. In: Boundary value problems for partial differential equations and applications, *RMA Res. Notes Appl. Math.*, vol. 29, pp. 99–111. Masson, Paris (1993)
13. Dullien, F.: Porous media. Academic Press San Diego (1979)
14. Durlofsky, L.J.: Numerical calculation of equivalent grid block permeability tensors for heterogeneous porous media. Water Resources Research **27**(5), 699–708 (1991)
15. E, W., Engquist, B., Li, X., Ren, W., Vanden-Eijnden, E.: Heterogeneous multiscale methods: a review. Commun. Comput. Phys. **2**(3), 367–450 (2007)
16. Efendiev, Y., Durlofsky, L.J.: Numerical modeling of subgrid heterogeneity in two phase flow simulations. Water Resources Research **38**(8) (2002)
17. Efendiev, Y., Ginting, V., Hou, T., Ewing, R.: Accurate multiscale finite element methods for two-phase flow simulations. J. Comput. Phys. **220**(1), 155–174 (2006)
18. Efendiev, Y., Pankov, A.: Numerical homogenization and correctors for nonlinear elliptic equations. SIAM J. Appl. Math. **65**(1), 43–68 (electronic) (2004)
19. Efendiev, Y.R., Hou, T.Y., Wu, X.H.: Convergence of a nonconforming multiscale finite element method. SIAM J. Numer. Anal. **37**(3), 888–910 (electronic) (2000)
20. Ergun, S.: Fluid flow through packed columns. Chemical Engineering Progress **48**, 89–94 (1952)
21. Ergun, S., Orning, A.: Fluid flow through randomly packed columns and fluidized beds. J. of Ind. Eng. Chem. **41** (1949)
22. Ewing, R.E., Lazarov, R.D., Lyons, S.L., Papavassiliou, D.V., Pasciak, J., Qin, G.: Numerical well model for non-darcy flow through isotropic porous media. Comput. Geosci. **3**(3-4), 185–204 (1999)
23. Ewing, R.E., Wang, J., Weekes, S.L.: On the simulation of multicomponent gas flow in porous media. Appl. Numer. Math. **31**(4), 405–427 (1999)
24. Fabrie, P., Langlais, M.: Mathematical analysis of miscible displacement in porous medium. SIAM J. Math. Anal. **23**(6), 1375–1392 (1992)
25. Forchheimer, P.: Wasserbewegung durch Boden. Zeit. Ver. Deut. Ing. (45), 1781–1788 (1901)
26. Fourar, M., Lenormand, R., Karimi-Fard, M., Horne, R.: Inertia effects in high-rate flow through heterogeneous porous media. Transport in Porous Media **60**, 353–370(18) (September 2005). DOI doi:10.1007/s11242-004-6800-6
27. Geertsma, J.: The effects of non-darcy flow on the behavior of hydraulically fractured gas wells. J. Pet. Tech. **883**, 1169 (1976)
28. Holden, L., Nielsen, B.F.: Global upscaling of permeability in heterogeneous reservoirs; the output least squares (ols) method. Transport in Porous Media **40**(2), 115–143 (2000)
29. Jikov, V.V., Kozlov, S.M., Oleinik, O.A.: Homogenization of differential operators and integral functionals. Springer-Verlag, Berlin (1994)
30. Jones, S.: Using the inertial coefficient beta to characterize heterogeneity in reservoir rock. In: SPE 16949 (1987)
31. L. S. Bennethum, T.G.: Generalized Forchheimer equation for two-phase flow based on hybrid mixture theory. Transport in Porous Media **26**(3), 261 – 275 (1997)
32. Lake, L.W.: Enhanced oil recovery. Prentice Hall (1989)
33. Marusić-Paloka, E., Mikelić, A.: The derivation of a nonlinear filtration law including the inertia effects via homogenization. Nonlinear Anal. **42**(1, Ser. A: Theory Methods), 97–137 (2000)
34. N. Frih Jean E. Roberts, A.S.: Modeling fractures as interfaces: A model for Forchheimer fractures. Computational Geosciences **2** (2008)
35. Narayanaswamy, G., Sharma, M.M., Pope, G.: Effect of heterogeneity on the non-darcy flow coefficient. SPE Reservoir Eval. & Engrg. **2**(3), 296–302 (1999)
36. Park, E.J.: Mixed finite element methods for generalized Forchheimer flow in porous media. Numer. Methods Partial Differential Equations **21**(2), 213–228 (2005)
37. Peaceman, D.W.: Fundamentals of numerical reservoir simulation, first edn. Elsevier Scientfic Publishing Company, Amsterdam-Oxford-New York (1977)
38. Peszyńska, M.: Mortar adaptivity in mixed methods for flow in porous media. International Journal of Numerical Analysis and Modeling **2**(3), 241–282 (2005)
39. Peszyńska, M., Jenkins, E., Wheeler, M.F.: Boundary conditions for fully implicit two-phase flow model. In: X. Feng, T.P. Schulze (eds.) Recent Advances in Numerical Methods for Partial Differential Equations and Applications, *Contemporary Mathematics Series*, vol. 306, pp. 85–106. American Mathematical Society (2002)

40. Peszyńska, M., Showalter, R.E.: Multiscale elliptic-parabolic systems for flow and transport. Electron. J. Differential Equations **2007**, No. 147, 30 pp. (electronic) (2007)
41. Peszynska, M., Trykozko, A., Augustson, K.: Computational modeling of inertia effects at porescale. In: Allen, Nabrzyski, Seidel, van Albada, Dongarra, and Sloot, (eds.) ICCS 2009 Proceedings, accepted (2009).
42. Peszyńska, M., Wheeler, M.F., Yotov, I.: Mortar upscaling for multiphase flow in porous media. Computational Geosciences **6**, 73–100 (2002)
43. Raviart, R.A., Thomas, J.M.: A mixed finite element method for 2nd order elliptic problems. In: Mathematical Aspects of the Finite Element Method, Lecture Notes in Mathematics, vol. 606, pp. 292–315. Springer-Verlag, New York (1977)
44. Reese, J.P., Long, K.R., Kelley, C.T., Gray, W.G., Miller, C.T.: Simulating non-darcy flow through porous media using sundance. In: P.J. Binning, P.K. Engesgaard, H.K. Dahle, G.F. Pinder, W.G. Gray (eds.) Proceedings of the XVI International Conference on Computational Methods in Water Resources (2006). URL http://proceedings.cmwr-xvi.org. Copenhagen, Denmark
45. Renard, P., de Marsily, G.: Calculating effective permeability: a review. Adv. Water Resour **20**, 253–278 (1997)
46. Russell, T.F., Wheeler, M.F.: Finite element and finite difference methods for continuous flows in porous media. In: R.E. Ewing (ed.) The Mathematics of Reservoir Simulation, pp. 35–106. SIAM, Philadelphia (1983)
47. Ruth, D., Ma, H.: On the derivation of the Forchheimer equation by means of the averaging theorem. Transport in Porous Media **7**(3), 255–264 (1992)
48. Zijl, W., Trykozko, A.: Numerical homogenization of the absolute permeability tensor around wells. SPE Journal. pp. 399–408 (2001)
49. Zijl, W., Trykozko, A.: Numerical homogenization of two-phase flow in porous media. Comput. Geosci. **6**(1), 49–71 (2002)